NASA CR-166721

RDS

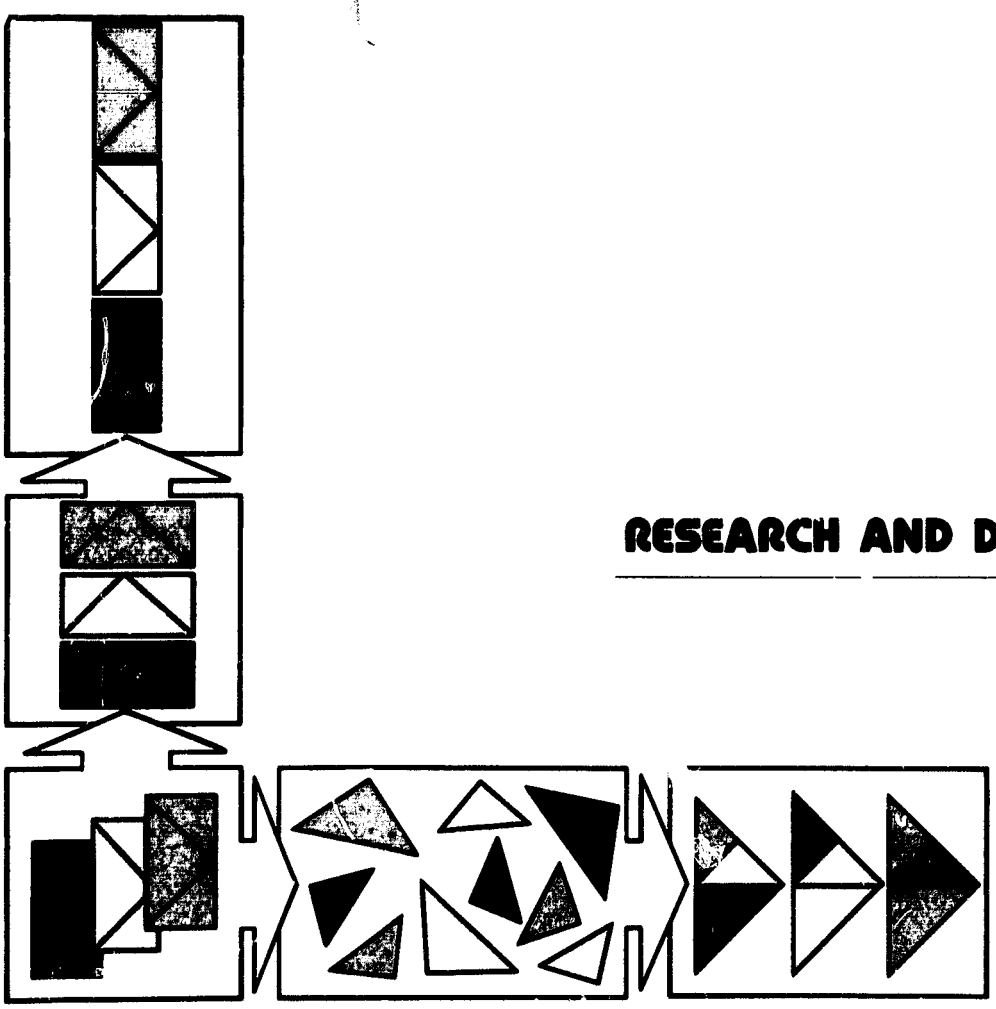

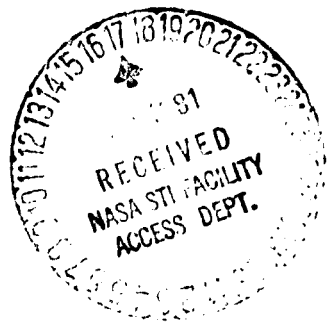

RESEARCH AND DATA SYSTEMS, INC.

SMMR DATA SET DEVELOPMENT FOR GARP

SMMR DATA SET DEVELOPMENT FOR GARP

PREPARED FOR

NATIONAL AERONAUTICS AND SPACE ADMINISTRATION
GODDARD SPACE FLIGHT CENTER
GREENBELT, MARYLAND 20771

UNDER
CONTRACT NO.: NAS 5-25781

MAY 1981

PREPARED BY

JOHN KOGUT

RESEARCH AND DATA SYSTEMS, INC.
9420 ANNAPOLIS ROAD
LANHAM, MARYLAND 20801

TABLE OF CONTENTS

1.0 INTRODUCTION

The NIMBUS-7 spacecraft was launched in October 1978 carrying eight instruments for observing the earth's atmosphere and oceans. One of these instruments is the Scanning Multichannel Microwave Radiometer (SMMR) which takes measurements of the microwave emission from the earth's atmosphere and surface at five frequencies from 6.6 GHz to 37.0 GHz and at two polarization modes for each frequency. The primary scientific objective of this instrument is to provide estimates of surface and atmospheric parameters of interest, based on the measured multispectral microwave radiances.

The tasks associated with this contract can be conveniently divided into two parts, concerned with the analysis of the NIMBUS-7 SMMR data. The tasks included in this contract are:

1. Evaluate the impact of cross polarization and Faraday rotation on SMMR-derived brightness temperatures.
2. Test and refine the algorithms used to retrieve the geophysical parameters and compare the retrieved parameters with values derived by other techniques.

The following sections of this report will describe the technical approach taken in each task, (Section 2.0) present the results from the tasks, (Section 3.0) and discuss the conclusions which can be drawn from this work (Section 4.0).

2.0 TECHNICAL APPROACH

2.1 SMMR Brightness Temperature Analysis

The SMMR instrument (Figure 2.1-1) provides orthogonally polarized antenna temperature measurements at five microwave frequencies 6.6 GHz, 10.7 GHz, 18.0 GHz, 21.0 GHz, and 37.0 GHz with an absolute accurate of less than 2°K (rms) at each frequency. The instrument employs Dicke type radiometers at all frequencies. At the four lower frequencies alternate polarizations are measured during successive scans of the SMMR antenna while at 37 GHz there is a radiometer operating continually at each polarization. The radiometers use an ambient RF termination and a horn antenna viewing deep space as a two point reference signal system. The main SMMR antenna is composed of a parabolic reflector illuminating a single feedhorn. The antenna main beam is offset 42° from nadir and scans the earth in a conical pattern with a half angle of about 25° (Figure 2.1-2). Additional SMMR performance characteristics are given in Table 2.1-I.

The SMMR data processing flow can be divided into three steps. The first step is composed of quality checks, conversion of radiometric data and earth location of each sensor field of view. The output of this step is an antenna temperature tape (TAT) containing about 19 orbits per tape. The second step is composed of the aggregation of individual fields of view into cells, application of polarization correction and sidelobe corrections and, the geographic location of each cell. The output of this step is a CELL tape containing about 6 days of data. The last step comprises the conversion of the average brightness temperatures, contained on the cell tape, to geophysical paramters. The output of this step is the so called PARM tape.

In this analysis the SMMR CELL tapes were used; only one set of calibration equations and coefficients are included in this data. This set is based on pre-launch laboratory tests and was the only set available at the time this study was completed. The CELL tape is constructed from the individual fields of view (FOV's) in the following way (see Figure 2.1-3). Each scan has a period 4.09 seconds and during this time the subsatellite point has progressed about 26.5 km (see the top picture of Figure 2.1-3). At an arbitrarily chosen time a grid is constructed as shown in the second picture of Figure 1. Each cell center and each

SMMR INSTRUMENT CONFIGURATION

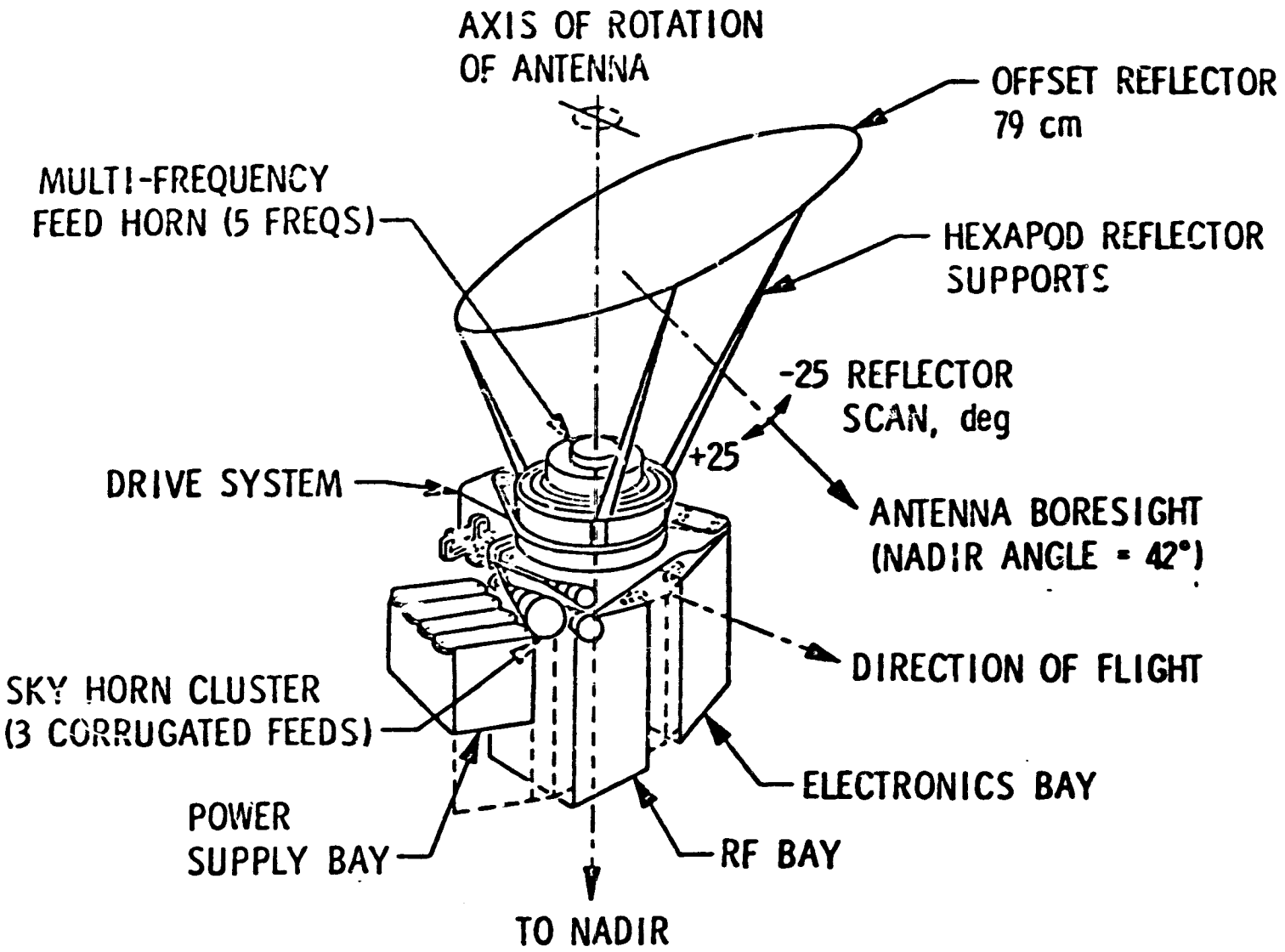

Figure 2.1-1

NIMBUS-G
SMMR SCAN GEOMETRY

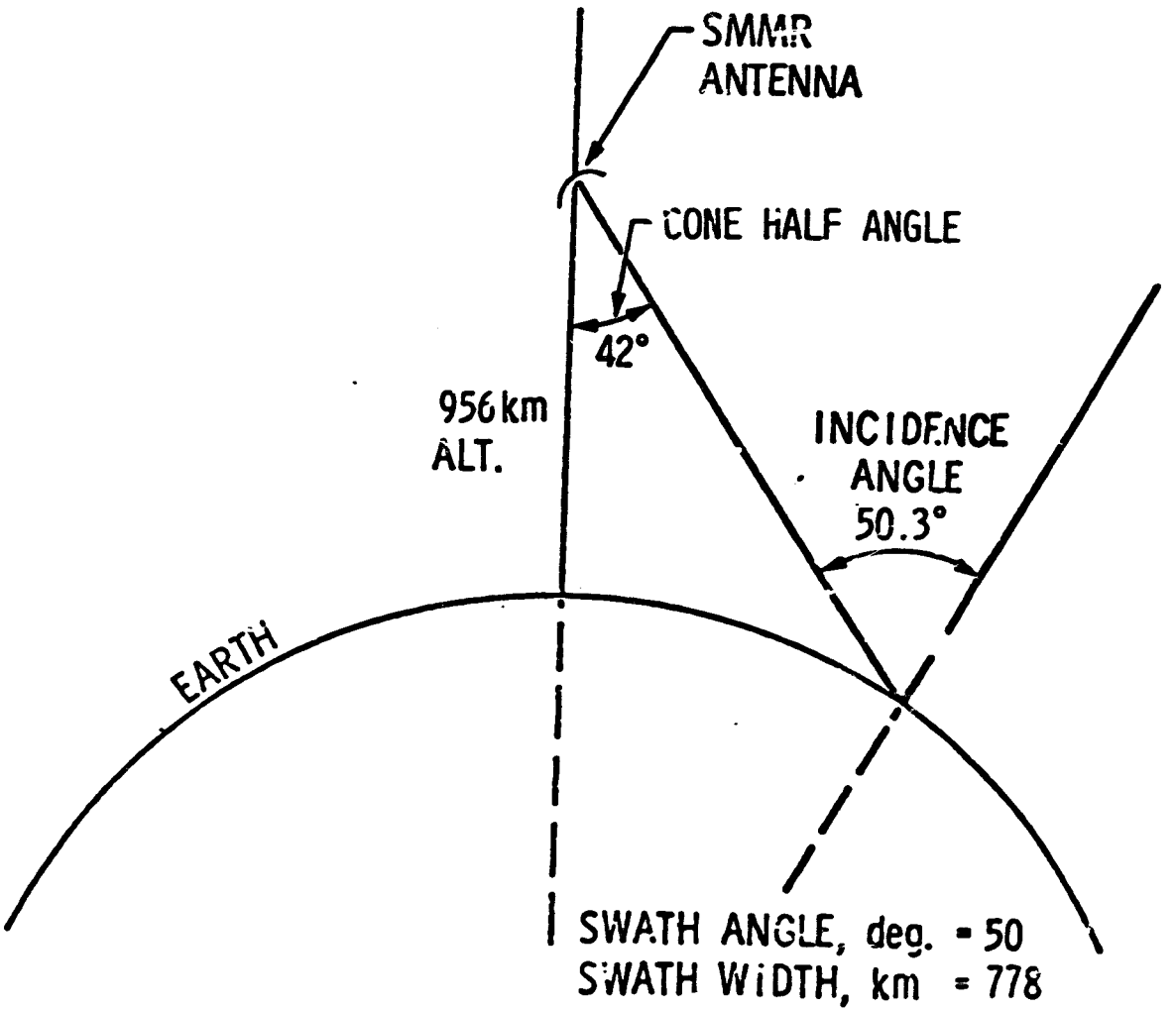

Figure 2.1-2

TABLE 2.1-I

SMMR PERFORMANCE CHARACTERISTICS

Parameter	Channel				
	1	2	3	4	5
Wavelength (cm)	4.54	2.8	1.66	1.36	0.81
Frequency (GHz)	6.6	10.69	18.00	21.00	37.00
R-F Bandwidth (MHz)	250	250	250	250	250
Integration Time (ms)(approximate)	126	62	62	62	30
I-F Frequency Range (MHz)	10-110	10-110	10-110	10-110	10-110
Dynamic Range (^{o}K)	10-330	10-330	10-330	10-330	10-330
Absolute Accuracy (^{o}K rms)	2.0	2.0	2.0	2.0	2.0
Temperature Resolution, ΔTrms (^{o}K)(per IFOV)	0.9	0.9	1.2	1.5	1.5
Antenna Beam Width ($\pm$0.2^{o})	4.2	2.6	1.6	1.4	0.8
Antenna Beam Efficiency (percent)	87.0	87.0	87.0	87.0	87.0
Scan Cycle $\pm$0.4 rad ($\pm$25^{o})/second	4.096	4.096	4.096	4.096	4.096
Double Sideband Noise (dB)(maximum)	5.0	5.0	5.0	5.0	5.0

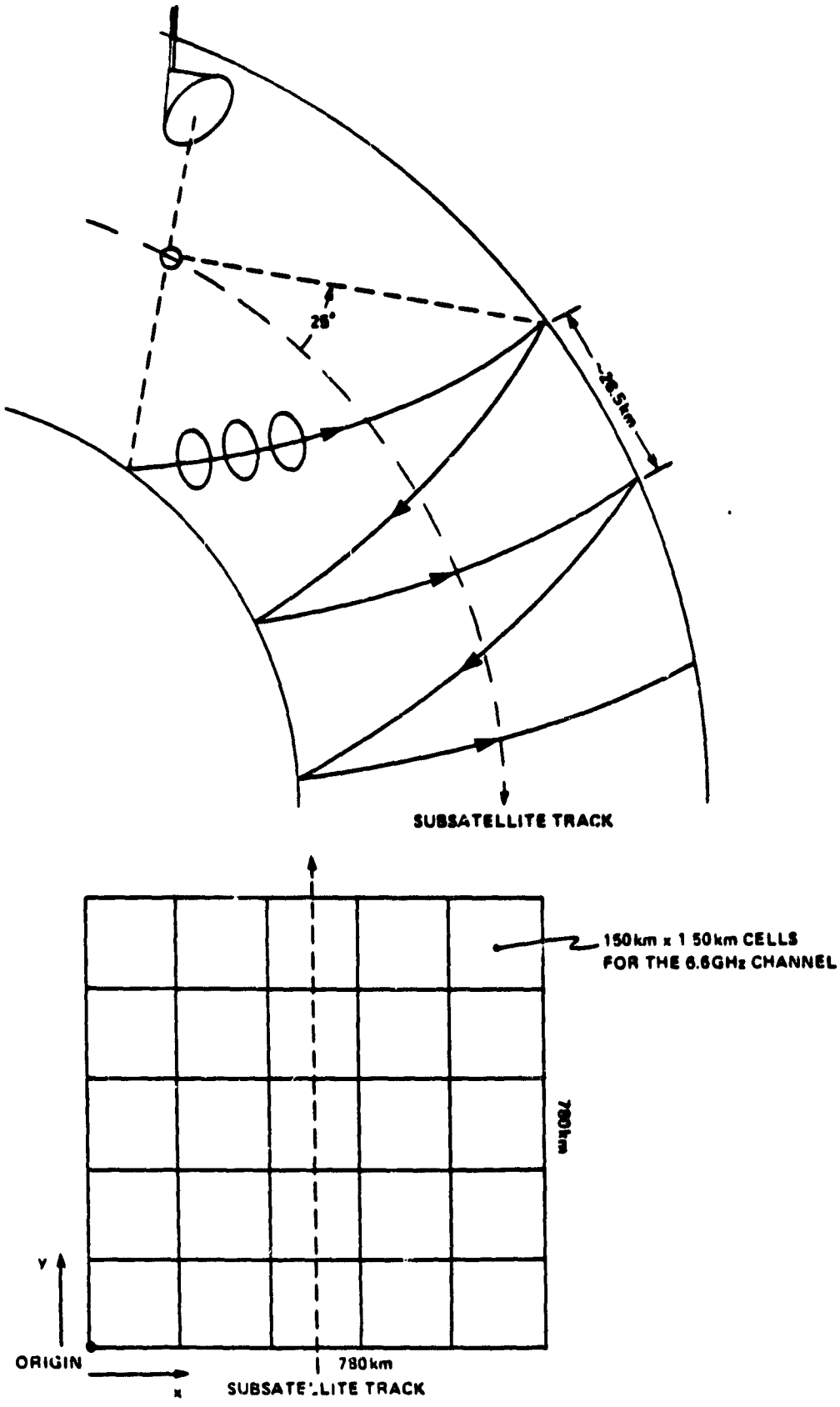
28°
~28.5km
SUBSATELLITE TRACK
150km x 150km CELLS
FOR THE 6.6GHz CHANNEL
780km
Y
ORIGIN
X
780km
SUBSATELLITE TRACK

FIGURE 2.1-3

FOV is tagged with an (x,y) location in this cartesian system. The boundaries of each cell are defined by the Δx, Δy distances from the cell center; for the 6.6 GHz channel $\Delta x = \Delta y = 75$ km. An FOV is included in a particular cell if $|x_{FOV} - x_c| \leq \Delta x$ and $|y_{FOV} - y_c| \leq \Delta y$. It turns out that about 30 scan periods are required to fill all the cells in a 780 km x 780 km block. Taking into account the 126 msec integration time and the ground track speed, it is seen that each cell will contain roughly 35 FOV's; these FOV's are then weighted and averaged over the cell.

The 10.7 GHz, 18.0 GHz, 21.0 GHz and 37.0 GHz observations are put into smaller cells in the 780 km by 780 km block since the resolution of the antenna is greater at these higher frequencies. Table 2.1-II gives the frequency and cell sizes of the brightness temperatures (T_b) available on the SMMR CELL-ALL tape. T_b measurements from the CELL tape were available for two time periods October 25 through November 25, 1978, and February 15 through March 17, 1979. Table 2.1-III shows the days during these time periods when good SMMR data was available for these tapes.

The main task in the analysis of the brightness temperatures was concerned with correcting the T_b's for polarization mixing between the horizontal and vertical components of the measured signal. The two months of SMMR brightness temperatures were averaged over the cells for each frequency and empirical correction factors for T_b to handle polarization mixing were computed for each frequency.

The Faraday rotation is an additional error caused by the motion of the dish with respect to the feed. The error in brightness temperature has been estimated to be as high as 1°K due to Faraday rotation. However, the empirical correction for cross polarization errors described earlier will compensate for the error due to Faraday rotation also.

TABLE 2.1-II FREQUENCY AND CELL SIZE OF OBSERVATIONS ON THE SMMR CELL-ALL TAPE

GRID	GRID SIZE (km)	BANDS X CELLS	CHANNELS INCLUDED IN GRID (GHz)
1	156.0	5 x 5	37.0, 21.0, 18.0, 10.7, 6.6
2	97.5	8 x 8	37.0, 21.0, 18.0, 10.7
3	60.0	13 x 13	37.0, 21.0, 18.0
4	30.0	26 x 26	37.0

TABLE 2.1-III SMMR DATA AVAILABLE ON THE CELL-ALL TAPES

	Day of Month																													
	1	2	3	4	5	6	7	8	9	10	11	12	13	14	15	16	17	18	19	20	21	22	23	24	25	26	27	28	29	30	3
October 1978	0	0	0	0	0	0	0	0	0	0	0	0	0	0	0	0	0	0	0	0	0	0	0	0	1	1	1	1	1	1	
November 1978	1	1	1	1	1	1	1	1	1	1	1	1	1	1	1	0	1	0	1	0	1	0	1	0	1	0	0	0	0	0	
February 1979	0	0	0	0	0	0	0	0	0	0	0	0	0	0	1	0	*	0	1	0	1	0	1	0	1	0	1	0			
March 1979	1	0	1	0	1	0	1	0	1	0	1	0	1	0	1	0	1	0	0	0	0	0	0	0	0	0	0	0			

0-No Data
1- Data
*-Bad Data

2.2 SMMR Algorithm Tests and Parameter Analysis

This part of the contract was concerned with evaluating the geophysical parameters which can be retrieved from the SMMR multispectral observations. The SMMR brightness temperatures, contained on the CELL tape, have been corrected for the effects of sidelobes and for mixing between the horizontal and vertical polarization components of the signal. However, analysis of the quality of the antenna and brightness temperatures must still be carried out; furthermore the calibration of this instrument has not been completed.

Several data sets were collected with the view in mind that these sets would be used to compare with the NIMBUS-7 SMMR geophysical parameter retrieval.

The NOAA environmental buoy data set covers the time period from January through April 1979. The data in this set come from 23 buoys located along the east and west coasts of the United States and in the Gulf of Mexico (see Figure 2.2-1 and Table 2.2-I).

The TIROS-N Advanced Very High Resolution Radiometer (AVHRR) is an infrared sensing instrument and the data set from this device covers the same time period as the buoy set. This set contains only sea surface temperature in earth located 50 km resolution cells; the absolute accuracy of this product is $\pm 1.5^{o}$ C.

Although two months of SMMR data have been made available for evaluation, only the month from February 15, 1979 to March 16, 1979 has been used in this analysis. This selection has been determined solely by the fact that the AVHRR data are not available to study the October-November 1978 SMMR data set.

Sea Surface Temperature (SST) statistics were constructed as follows:

1. a thirty day mean and standard deviation were computed at each buoy for the February-March data.
2. all AVHRR SST's which fell within a $\pm 1^{o}$ x $\pm 1^{o}$ block, centered on each buoy, were used to compute a mean and standard deviation for the same time period.
3. step (2) was carried out for the SMMR SST's with the added constraint that if the rain rate in a particular cell exceeded 1 mm/hr the SST was not included in the statistics.

FIGURE 2.2-1

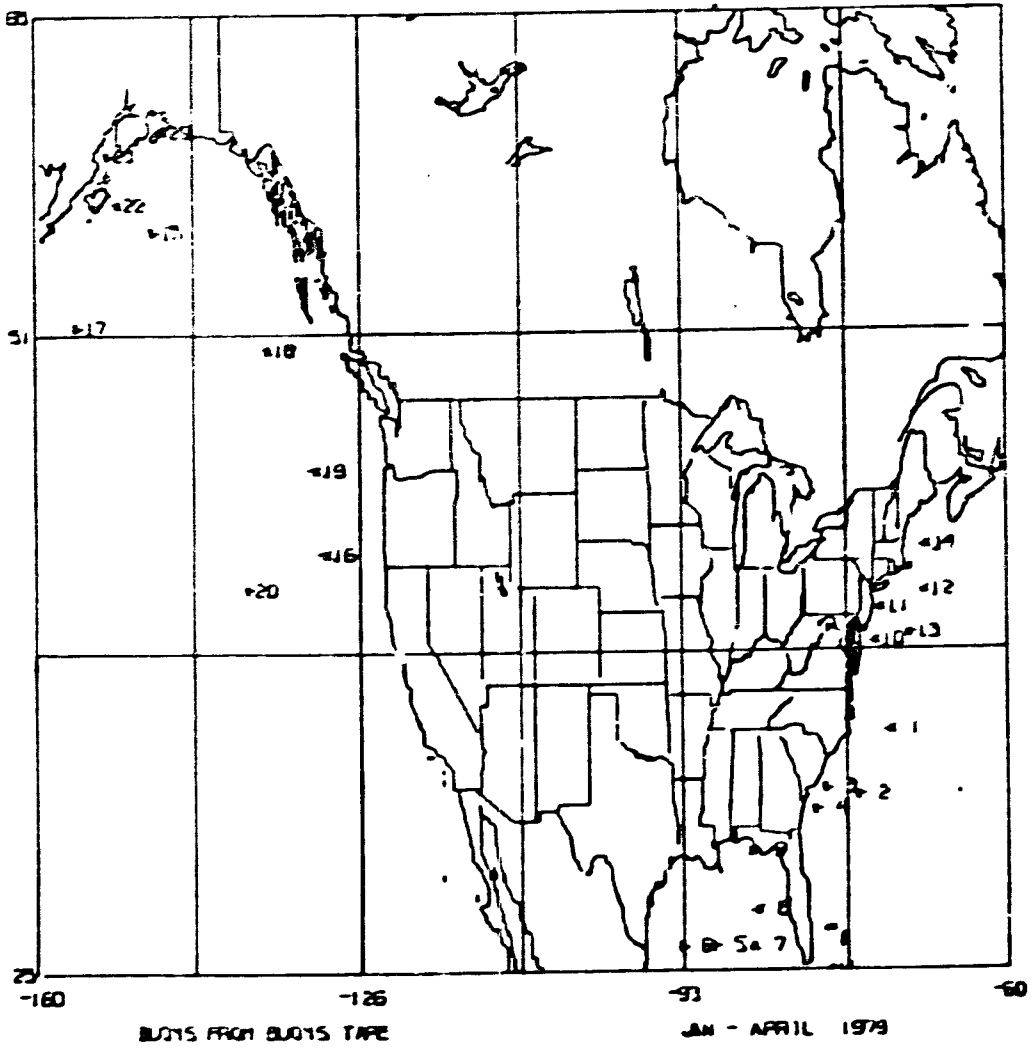

TABLE 2.2-I

POSITIONS AND FREQUENCY OF OBSERVATIONS

FOR THE BUOYS ON THE BUOY TAPE

BUOY NUMBER	LATITUDE (°N)	LONGITUDE (°W)	FREQUENCY OF OBSERVATIONS (HRS)
1	35.0	72.0	3
2	32.3	75.3	1
3	32.6	78.7	1
4	31.7	79.7	1
5	26.0	90.0	3
6	26.0	93.5	1
7	26.0	86.0	3
8	27.5	85.5	4
9	30.0	85.9	3
10	38.7	73.6	1
11	40.1	73.0	1
12	40.8	68.5	3
13	39.0	70.0	3
14	42.7	68.3	3
15	56.0	148.0	3
16	42.5	130.0	3
17	52.0	156.0	1
18	51.0	136.0	3,1
19	46.0	131.0	1
20	41.0	138.0	3
21	59.2	152.7	3
22	57.1	151.7	3
23	60.2	146.8	1

4. the SMMR SST product was decomposed into day and night passes.

In addition a comparison was made of the SMMR and AVHRR SST retrievals in open ocean areas at various latitudes.

Near the beginning of 1981 a new set of SMMR CELL tapes were made available. The brightness temperatures on these new tapes reflect an improvement to the antenna pattern correction model used to compute brightness temperature from the SMMR antenna temperatures. Some comparisons of the sea surface temperatures retrieved using these new brightness temperatures and AVHRR SST's were also made.

In all of the geophysical parameter retrievals from the SMMR brightness tempeature the algorithms described in Wilheit and Chang 1980 were used.

The results of the SMMR SST retrieval and comparison are described in Section 3.2.

3.0 RESULTS

3.1 Brightness Temperature Analysis

The brightness temperatures given on the SMMR CELL-ALL tape in general incude the effects of an unknown polarization mixing between the vertically polarized and horizontally polarized components of the signal received by the SMMR antenna. Any pair of brightness temperatures for a cell $\begin{pmatrix} T_{v'} \\ T_{h'} \end{pmatrix}$ are related to the true brightness temperatures $\begin{pmatrix} T_v \\ T_h \end{pmatrix}$ by a matrix representing the effects of polarization mixing as follows:

$$\begin{pmatrix} T_{v'} \\ T_{h'} \end{pmatrix} = \begin{pmatrix} A & C \\ D & B \end{pmatrix} \begin{pmatrix} T_V \\ T_h \end{pmatrix} \qquad (1)$$

Here C=1-A and D=1-B since the radiometer was calibrated using an unpolarized source. If A+B=1, we can invert this matrix to determine the true brightness temperatures, giving:

$$\begin{pmatrix} T_v \\ T_h \end{pmatrix} = \begin{pmatrix} \alpha & \gamma \\ \delta & \beta \end{pmatrix} \begin{pmatrix} T_{v'} \\ T_{h'} \end{pmatrix} \qquad (2)$$

Since the antenna coordinate system is skewed with respect to the conventional surface polarization coordinate system, the polarization mixing can be represented by a coordinate transformation of the type:

$$\begin{pmatrix} T_v \\ T_h \end{pmatrix} = \begin{pmatrix} \alpha & 1-\alpha \\ 1-\beta & \beta \end{pmatrix} \begin{pmatrix} T_{v'} \\ T_{h'} \end{pmatrix} \qquad (3)$$

If the true brightness temperatures were known for an observation at a particular scan position; α and β for this case could be determined. Although the true brightness temperatures cannot be measured, we can assume; considering the cause of the polarization mixing, that this mixing has the smallest effect at the center cell of the 780 km by 780 km SMMR block. We may then take the center cell of the 5 x 5, 156 km resolution grid as the cell in which the least polarization mixing occurs, and thus as the standard from which the compute the relative correction terms for polarization mixing. We may also assume that on the average, the data from the other scan positions which contribute to the cells on either side of the center cell, should on the global average, have the same brightness temperatures at all resolutions as the off center cells in the 156 km resolution case.

For a given frequency, cell number, and grid size, we can then solve for α and β to give:

$$\alpha = \frac{T_v - T_h'}{T_v' - T_h'}$$

$$\beta = \frac{T_h - T_v'}{T_h' - T_v'} \qquad (4)$$

Since the center cell (number 3) for the 156 km resolution is used as the standard for these computations, for all frequencies at this grid size, $\alpha = \beta = 1$.

The correction terms α and β were computed from the SMMR CELL-ALL tape in the following manner. To eliminate cases of land in the field of view, α and β were computed for a cell only if T_h' was less than 200°K. To minimize the effects of Faraday rotation and to eliminate sun glint from the observations, α and β for a cell were computed only if the day/night/twilight indicator on the CELL-ALL tape for the band which contained the cell indicated that the band was in the dark. In addition, brightness temperatures less than 60°K were rejected, and only cells which were between $\pm 50^\circ$ latitude were included in the computations.

If the brightness temperatures for a cell satisfied the above conditions, α and β for the cell were computed for all the appropriate frequencies at the 156 km, 97.5 km, 60 km, and 30 km resolutions. For all resolutions the brightness temperatures of cell number 3 in the 156 km resolution case were used for T_v and T_h in equation (4). All the individual values for α and β were then summed and averaged to obtain the final polarization correction terms.

The two months of SMMR T_b observations were divided into time groups. Group 1 covered October 25 to November 9, 1978 and contained 16 days of SMMR observations, Group 2 covered November 10 to November 25, 1978 and contained 11 days of SMMR T_b's, and Group 3 covered February 15 through March 17, 1979 and contained 15 days of SMMR data. Correction factors for each frequency were computed for the observations in Group 1 and then applied to the data in all three groups. Averages of the corrected data were taken in the down track direction for each cell, and plots were made of the corrected T_b's for the 156 km resolution data for both polarizations (Figure 3.1-1 to Figure 3.1-5). We can see from these figures that the variations across the scan range from a few tenths of a degree to 1.5°K which gives an improvement over a cross track bias of 5-8°K for uncorrected data.

Figure 3.1-6 shows the difference between the cross track and along track averages for the 6.6 GHz data. These averages should have the same value, and the 0.5°K difference is due mainly to noise in the data.

FIGURE 3.1-1

CORRECTED BRIGHTNESS TEMPERATURE AVERAGES

37 GHz ALONG TRACK AVERAGE

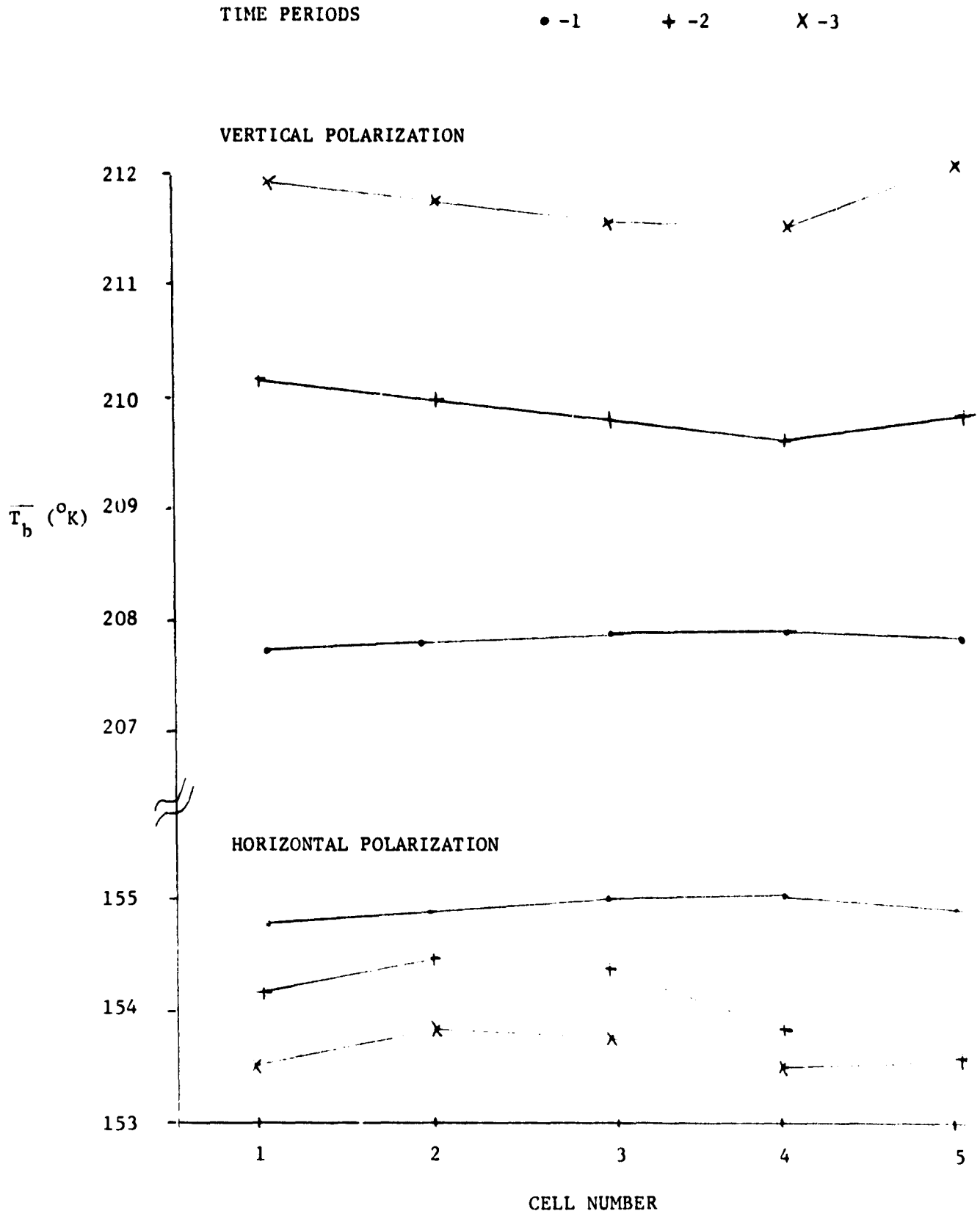

FIGURE 3.1-2

CORRECTED BRIGHTNESS TEMPERATURES AVERAGES

21 GHz ALONG TRACK AVERAGE

TIME PERIODS

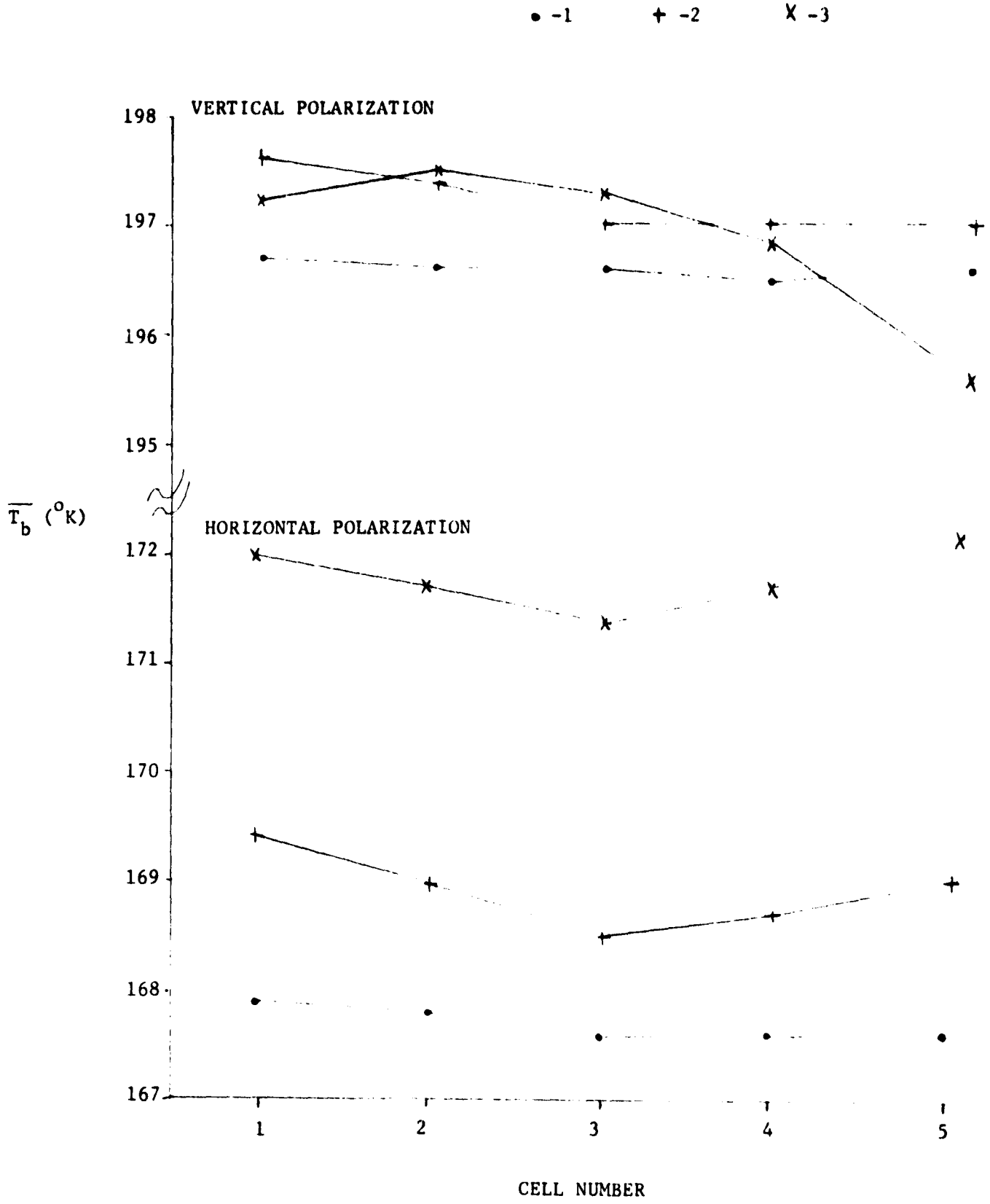

FIGURE 3.1-3

CORRECTED BRIGHTNESS TEMPERATURE AVERAGES

18 GHz ALONG TRACK AVERAGE

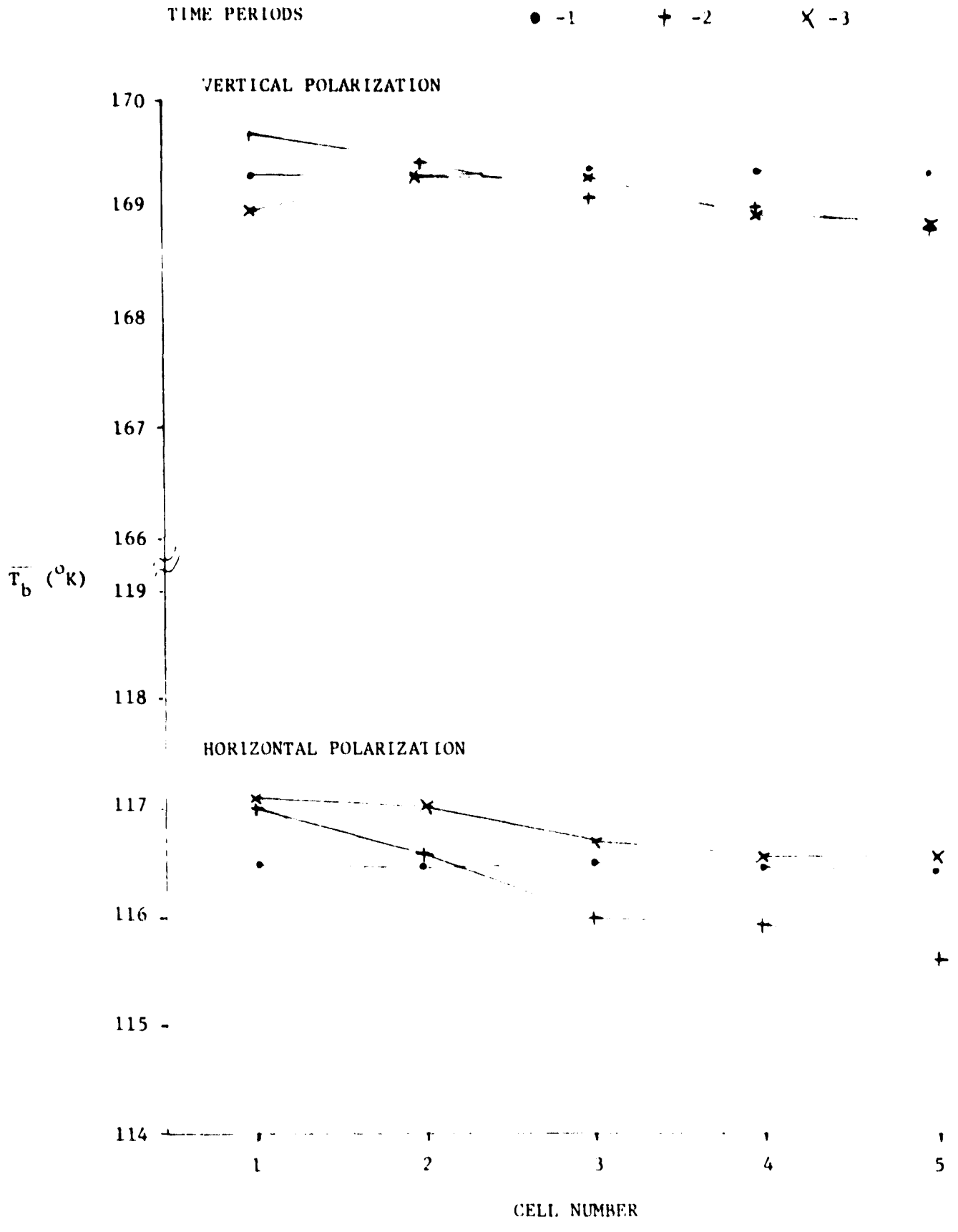

FIGURE 3.1-4

CORRECTED BRIGHTNESS TEMPERATURE AVERAGES

11 GHz ALONG TRACK AVERAGE

TIME PERIODS ● -1 + -2 × -3

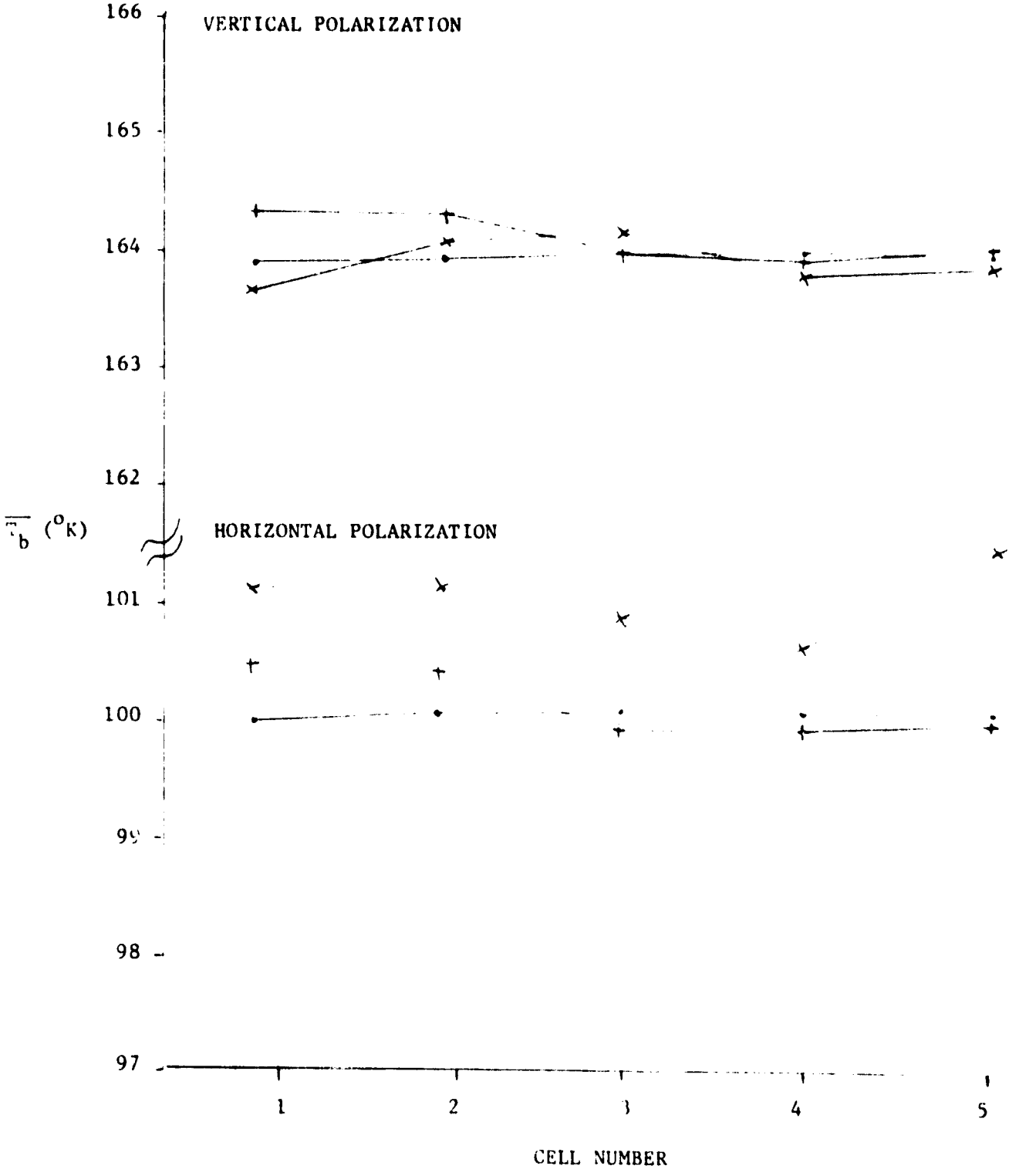

FIGURE 3.1-5

CORRECTED BRIGHTNESS TEMPERATURE AVERAGES

6.6 GHz ALONG TRACK AVERAGE

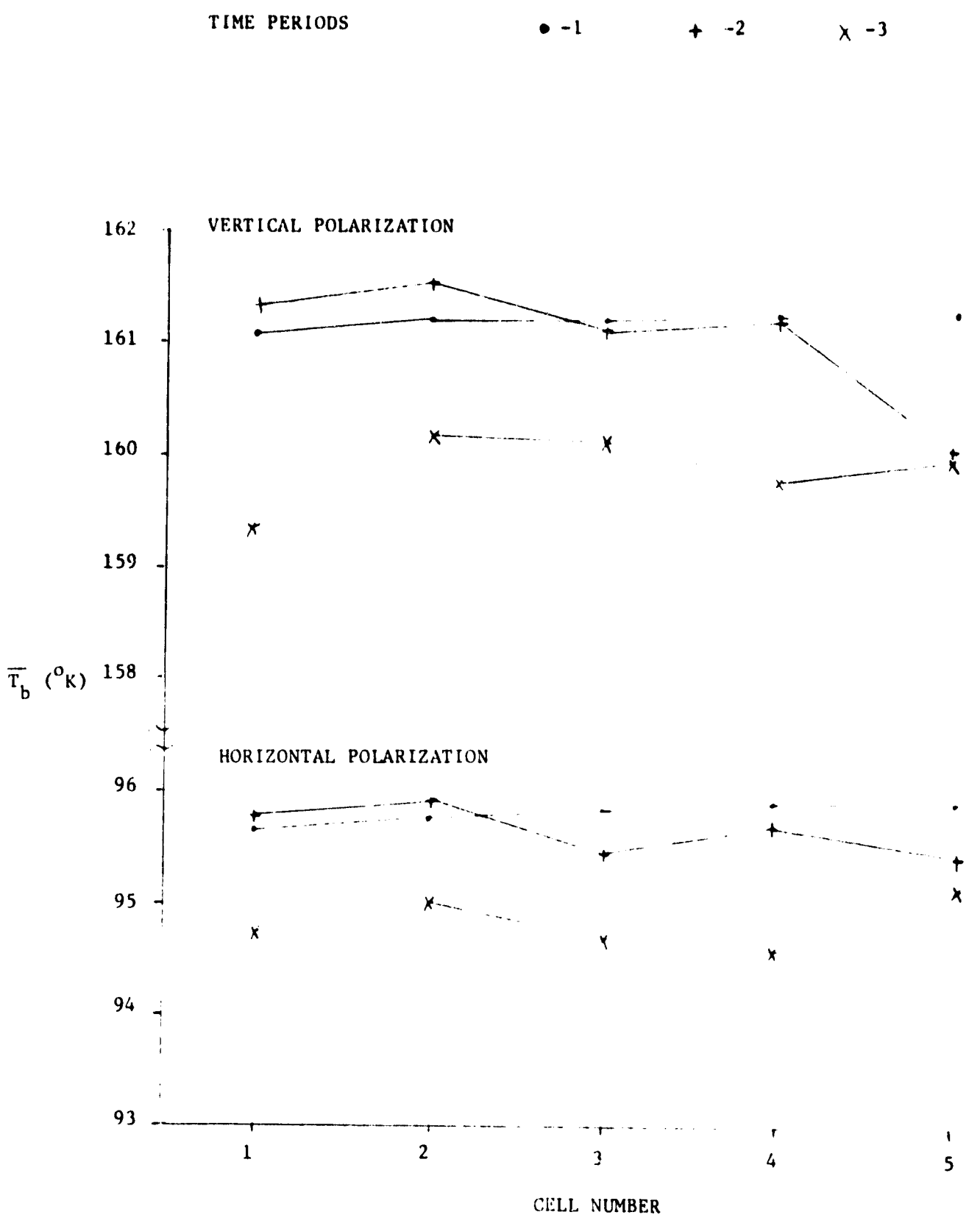

FIGURE 3.1-6

CORRECTED BRIGHTNESS TEMPERATURE AVERAGES

6.6 GHz TIME PERIOD J

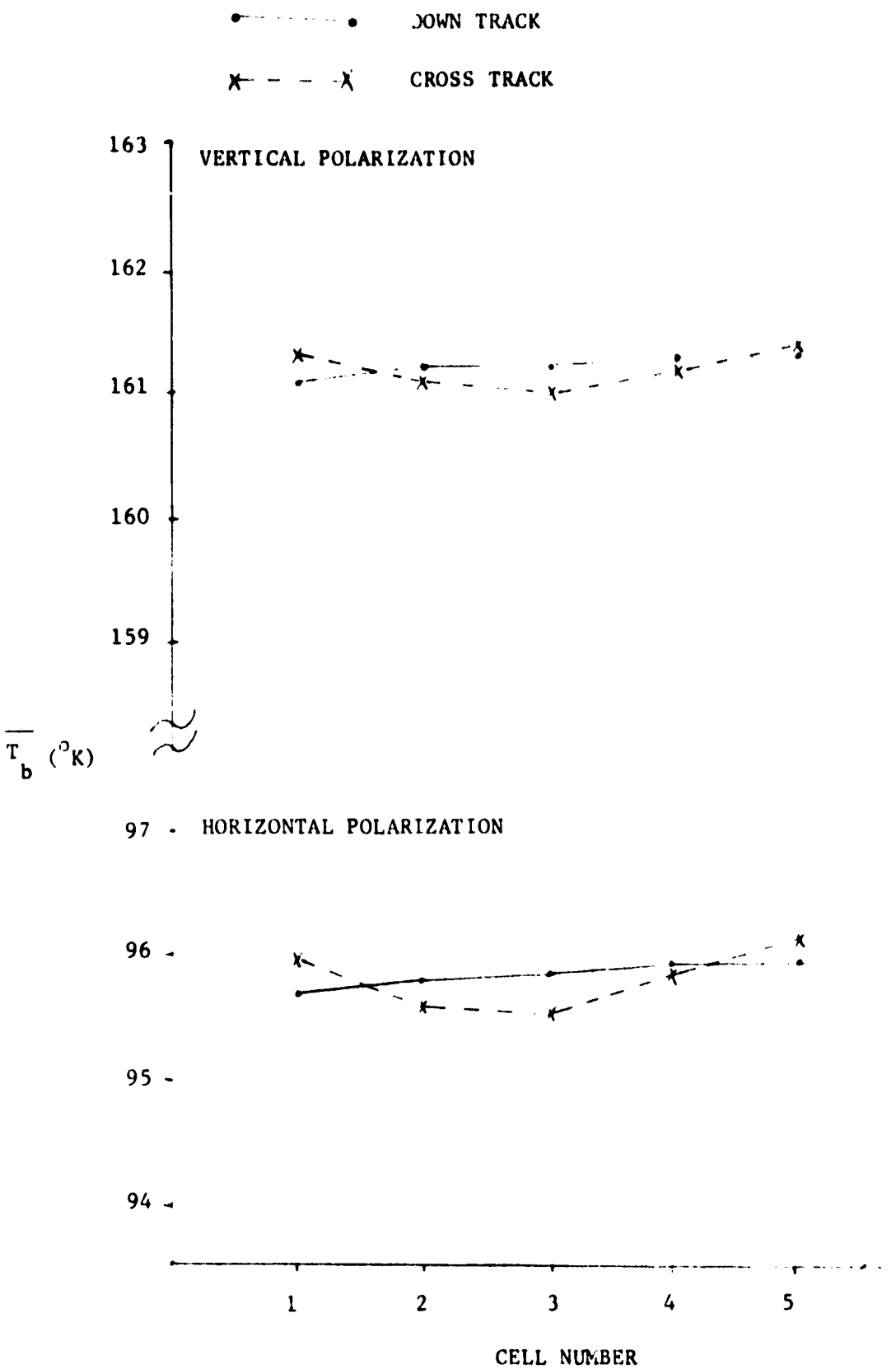

3.2 SMMR Algorithm Test and Parameter Comparison

The results for the comparison of the buoy, AVHRR and SMMR sea surface temperature statistics for the February-March 1979 time period are shown in Table 3.2-I. Here SST denotes the mean sea surface temperature in ^{o}C, σ is the standard deviation of the respective data, and POP denotes the number of observations. In addition,

$$\Delta_A = SST_B - SST_A$$
$$\Delta_D = (SST_B - SST_S)_{DAY}$$
$$\Delta_N = (SST_B - SST_S)_{NIGHT}$$

It is immediately noticed how tight the population is at each buoy, with the exception of buoy 13; the standard deviations are consistently less than $1^{o}C$. The mean of all buoy standard deviations is $0.6^{o}C$. The AVHRR data shows a wider distribution centered around each buoy. The AVHRR standard deviation is greater than the buoy standard deviation in 13 of the 16 cases in which coincident data is available; the mean of the AVHRR standard deviation is $1.1^{o}C$, about twice that for the buoys. This is most likely caused by the way we've chosen to compute the statistics e.g. by defining $\pm 1^{o}$ squares centered on each buoy. In particular look at buoy 17, it lies west of Ocean Station PAPA and is located between the Subartic Current to the south and the Alaskan Current to the north. The AVHRR sample distribution about this buoy is four times wider than the sample distribution from buoy 17. It is felt that this is so because of the larger variation of temperature in a roughly 250 km x 250 km area centered at buoy 17. A similar comment can be made about buoy 20 where the AVHRR sample distribution is twice as wide as the distribution at buoy 20. It is recalled that buoy 20 also is located in a region of intense oceanic activity; it lies about 1500 km off the coast of northern California in a region where North Pacific Current and the California Current meet and reinforce each other.

In the case of SMMR, it is seen that the statistical distributions are much wider than the buoy distributions. This is due, in large part, to the inherent spatial resolution of this instrument which leads to one, and sometimes, two orders of magnitude reduction in the population of observations. Consequently very little smoothing of the observations is done.

TABLE 3.2-I

BUOY-AVHRR-SMMR MEAN SEA SURFACE TEMPERATURE COMPARISON 2/15-3/16, 1979

			BUOY			AVHRR				SMMR DAY				SMMR NIGHT			
BUOY	LAT(°N)	LON(°W)	$\overline{SST}$	σ	POP	$\overline{SST}$	σ	POP	Δ_A	$\overline{SST}$	σ	POP	Δ_D	$\overline{SST}$	σ	POP	Δ_N
1	35.0	72.0	----	---	---	19.8	0.9	95	---	15.7	2.2	6	---	21 7	2.7	11	---
2	32.3	75.3	20.9	0.7	711	21.8	1.3	153	-1.1	17.9	2.5	7	3.0	23.4	3.9	10	-3.5
3	32.6	78.7	18.1	1.7	712	22.3	1.6	153	-4.2	18.1	0.0	1	0.0	18.8	0.0	1	-0.7
4	31.7	79.7	----	---	---	23.2	2.0	123	---	----	---	-	---	----	---	--	---
5	26.0	90.0	20.9	0.6	348	22.1	0.8	182	-1.2	26.0	5.6	9	-5.1	23.2	1.7	6	-3.7
6	26.0	93.5	20.1	0.6	716	21.8	0.6	162	-1.7	24.5	2.8	10	-4.4	----	---	-	---
7	26.0	86.0	25.8	0.4	242	25.1	1.0	226	0.7	25.2	2.9	8	0.6	25.5	1.8	5	0.3
8	27.5	85.5	----	---	---	23.1	1.3	217	---	21.7	4.3	8	---	21.3	2.8	4	---
9	30.0	85.9	14.2	0.6	24ن	20.3	0.7	28	-6.1	----	---	-	---	----	---	-	---
10	38.7	73.6	----	---	---	9.6	1.7	53	---	5.8	0.0	1	---	----	---	-	---
11	40.1	73.0	4.5	0.4	717	7.4	1.4	22	-2.9	----	---	-	---	----	---	-	---
12	40.8	68.5	----	---	---	11.5	3.8	16	---	5.3	3.6	4	---	11.8	5.0	4	---
13	39.0	70.0	12.8	2.0	241	14.0	2.2	87	-1.2	8.1	2.7	6	4.7	15.7	4.3	8	-2.9
14	42.7	68.3	3.8	0.5	235	4.0	1.3	29	-0.2	----	---	-	---	7.2	1.2	2	-3.4
15	56.0	148.0	3.6	0.1	241	3.4	0.3	88	0.2	12.2	2.0	5	-8.6	23.7	33.5	3	-20.3
16	42.5	130.0	11.5	0.2	240	11.4	0.4	132	0.1	12.0	1.7	9	-0.5	10.8	6.9	6	0.7
17	52.0	156.0	3.5	0.1	713	3.4	0.4	46	0.1	5.3	2.6	6	-1.8	0.3	0.4	2	3.2
18	51.0	136.0	6.3	0.2	498	7.0	0.5	138	-0.7	12.5	2.2	5	-6.2	6.2	5.2	8	0.1
19	46.0	131.0	8.8	0.3	715	9.3	0.5	134	-0.5	10.8	1.1	8	-2.0	12.9	5.3	9	-4.1
20	41.0	138.0	11.3	0.3	242	11.9	0.6	134	-0.6	9.1	0.9	6	2.2	8.7	3.1	10	2.6
21	59.2	152.7	3.8	0.5	203	----	---	---	---	----	---	-	---	----	---	-	---
22	57.1	151.7	----	---	---	3.6	0.5	66	---	----	---	-	---	----	---	-	---
23	60.2	146.8	2.8	0.4	714	4.1	0.2	11	-1.3	----	---	-	---	----	---	-	---
				$\overline{\sigma}=0.6$			$\overline{\sigma}=1.1$		$\overline{\Delta}_A=1.4$		$\overline{\sigma}=2.6$		$\overline{\Delta}_D=3.3$		$\overline{\sigma}=3.4$		$\overline{\Delta}_N=2.3$

$\overline{SST}$, σ, and Δ_A, Δ_D, Δ_N are in °C

Using the buoy data as the standard, it is seen in Table 3.2-I that the buoy/AVHRR comparison yields a mean difference of -1.3°C. However, there are three buoys where Δ_A is greater than 2.5°C and two of these locations shows a sparse AVHRR population (#'s 9 and 11). The third of these locations (#3) is off the coast of South Carolina directly east of Charleston and lies in the region where the Gulf Stream impinges upon the shelf water; consequently large changes in temperature over a month can occur in a $\pm 1^{\circ} \times \pm 1^{\circ}$ square centered on the buoy.

A comparison of the SMMR and buoy data shows an even greater deviation from the buoy data. The mean difference of the daytime data is -1.5°C and the nighttime data shows a mean Δ_N of -1.0°C. A comparison of the SMMR daytime and nighttime data shows very large deviations in SST; of the 14 locations in which there are coincident daytime and nighttime data, the nighttime SST exceeded the daytime SST eight times. Moreover the nighttime data exceeded the daytime data by an average of 5.0°C; in those 6 cases in which the daytime results exceeded the nighttime results the average difference was 2.0°C.

It has been proposed that the SMMR SST retrievals may be affected by the problem of land/ocean boundaries within the footprint and may also be affected by radio frequency interference from terrestrial transmitters along coastlines. To test this hypothesis a number of mid-ocean areas were chosen in which SMMR retrievals were compared with AVHRR retrievals. The mid-ocean test areas are shown in Figure 3.2-1.

The AVHRR statistics for each $\pm 1^{\circ} \times \pm 1^{\circ}$ block in each test area were computed; the SMMR statistics were computed using a $\pm 2^{\circ} \times \pm 2^{\circ}$ grid because the SST for this instrument is computed at 156 km resolution. Furthermore, the statistics were screened for rain rates greater than 1 mm/hour and a geography filter for each observation was checked to make sure only ocean data was included in the statistics. To make the data more geographically compatible the AVHRR SST's for each $\pm 1^{\circ} \times \pm 1^{\circ}$ block were averaged into $\pm 2^{\circ} \times \pm 2^{\circ}$ blocks; each of these smaller blocks were in turn accumulated and averaged so as to make the $20^{\circ} \times 20^{\circ}$ ocean test areas. The results are shown in Table 3.2-II. In addition to this table the SST differences were contoured at 1°C intervals and also plotted; the plotted and contoured informatin is shown in Figures 3.2-2 through 3.2-5.

FIGURE 3.2-1

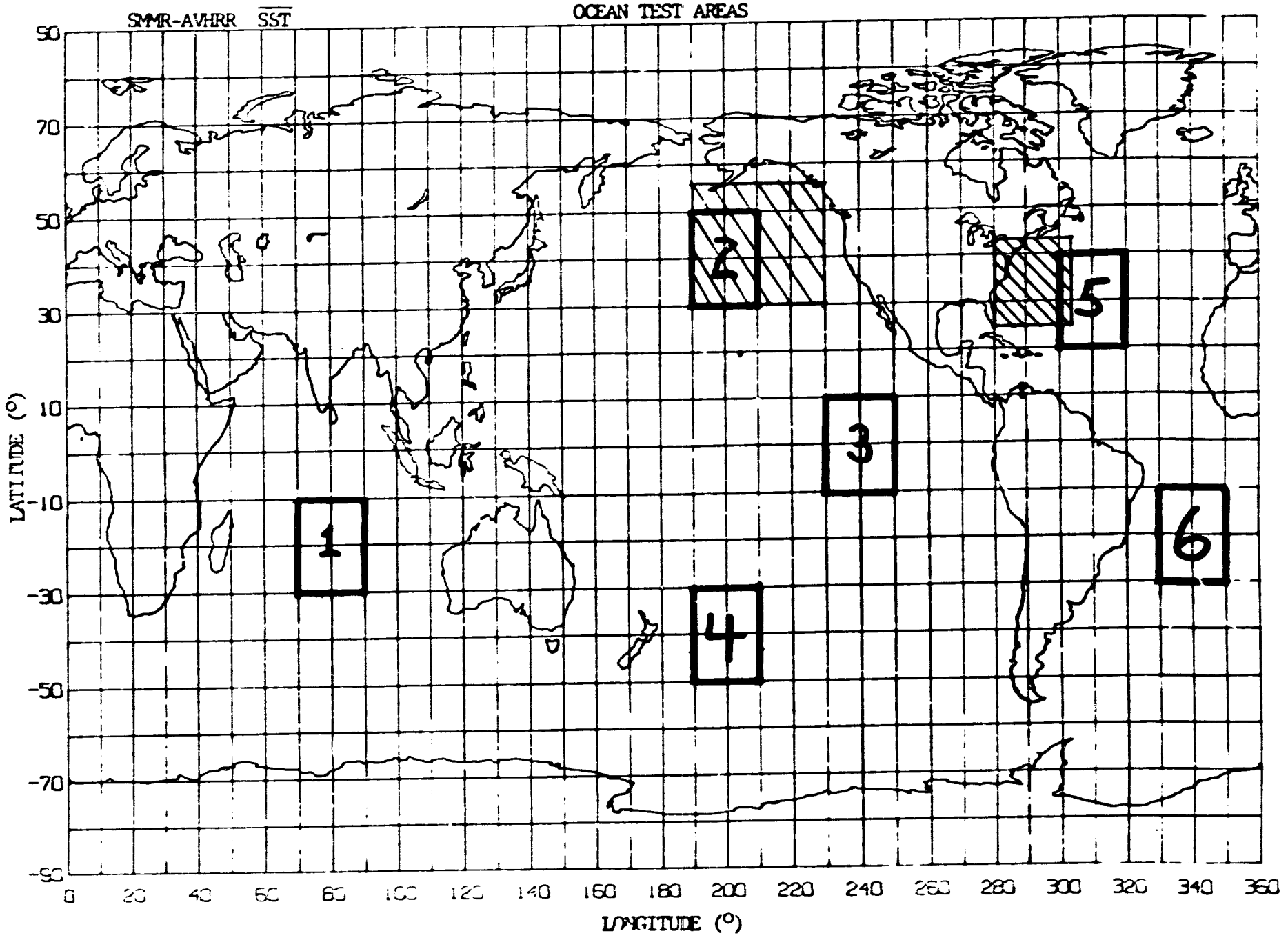
SMMR-AVHRR $\overline{SST}$
OCEAN TEST AREAS
90
70
50
30
10
-10
-30
-50
-70
-90
LATITUDE (°)
0
20
40
60
80
100
120
140
160
180
200
220
240
260
280
300
320
340
360
LONGITUDE (°)
1
2
3
4
5
6

TABLE 3.2-II

SMMR-AVHRR SST COMPARISON FOR SIX OPEN OCEAN AREAS FEB 15-MAR 16, 1979

AREA	LATITUDE	LONGITUDE	AVHRR SST				SMMR SST				(SMMR-AVHRR) SST		
			$\overline{SST}$(°C)	σ(°C)	POP		$\overline{SST}$(°C)	σ(°C)	POP	$\overline{SST}$(°C)	σ(°C)	POP
1	30°S-10°S	70°E-90°E	25.5	1.4	386	DAY	21.6	2.0	100	-4.0	-1.3	100
						NIGHT	23.4	2.4	96	-2.3	2.0	96
2	30°N-50°N	170°W-150°W	11.1	4.4	400	DAY	7.7	3.8	100	-3.4	1.3	100
						NIGHT	7.2	3.6	100	-3.8	1.5	100
3	10°S-10°N	130°W-110°W	26.2	0.5	391	DAY	23.4	0.9	100	-2.7	1.0	100
						NIGHT	21.0	1.2	100	-5.2	1.3	100
4	50°S-30°S	170°W-150°W	19.1	3.3	400	DAY	16.4	3.5	100	-2.7	0.8	100
						NIGHT	14.7	3.0	100	-4.4	0.7	100
5	20°N-40°N	60°W-40°W	20.3	2.5	400	DAY	16.5	3.3	100	-3.8	1.3	100
						NIGHT	17.3	2.4	100	-3.0	1.6	100
6	30°S-10°S	30°W-10°W	25.2	0.6	397	DAY	20.0	1.0	100	-5.2	1.0	100
						NIGHT	22.7	1.5	54	-2.3	1.2	54

FIGURE · 3.2-2

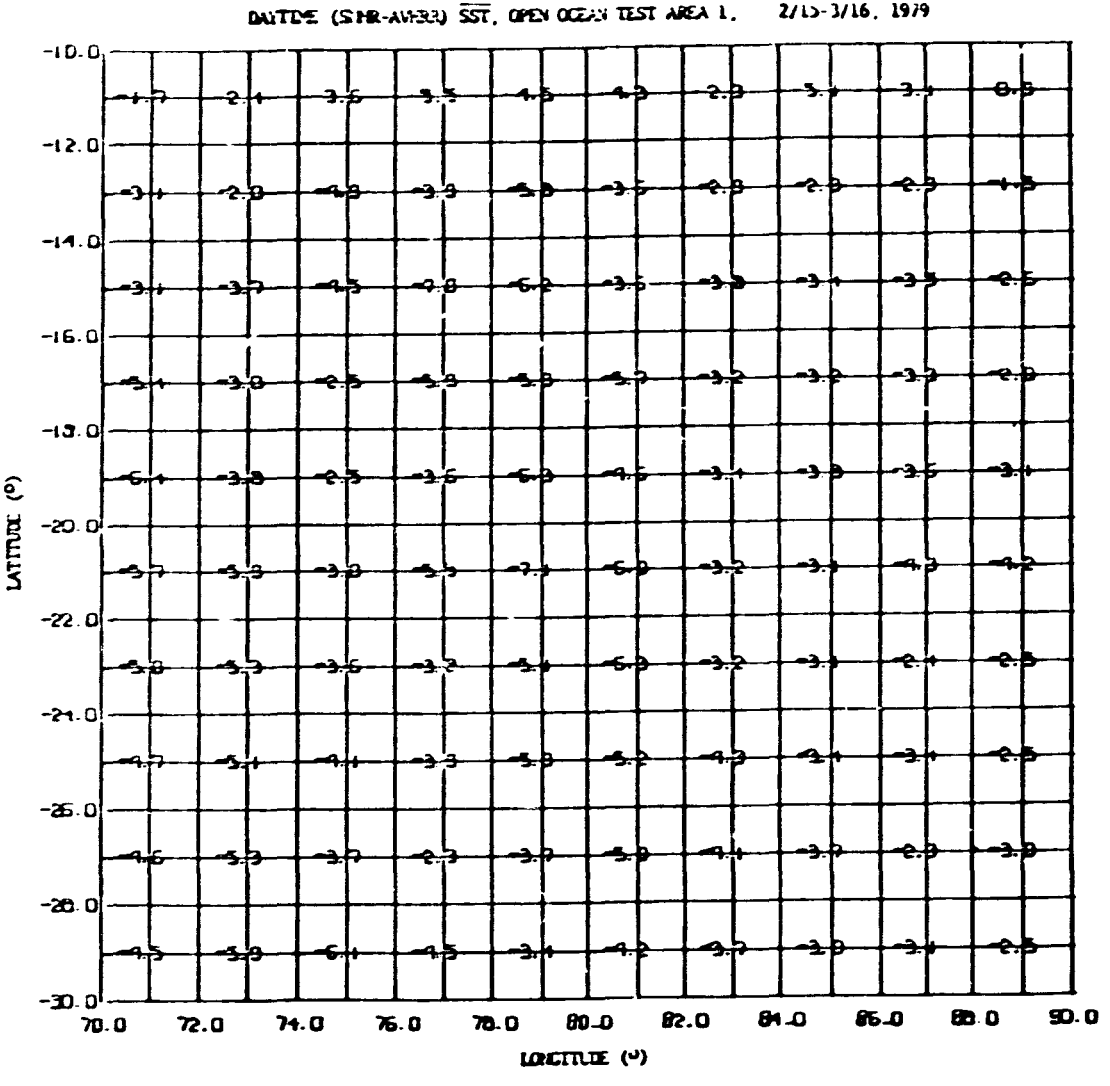
DAYTIME (SIX-HR-AVERAGE) SST, OPEN OCEAN TEST AREA 1. 2/15-3/16, 1979
-10.0
-12.0
-14.0
-16.0
-18.0
-20.0
-22.0
-24.0
-26.0
-28.0
-30.0
LATITUDE (°)
70.0
72.0
74.0
76.0
78.0
80.0
82.0
84.0
86.0
88.0
90.0
LONGITUDE (°)

FIGURE 3.2-3

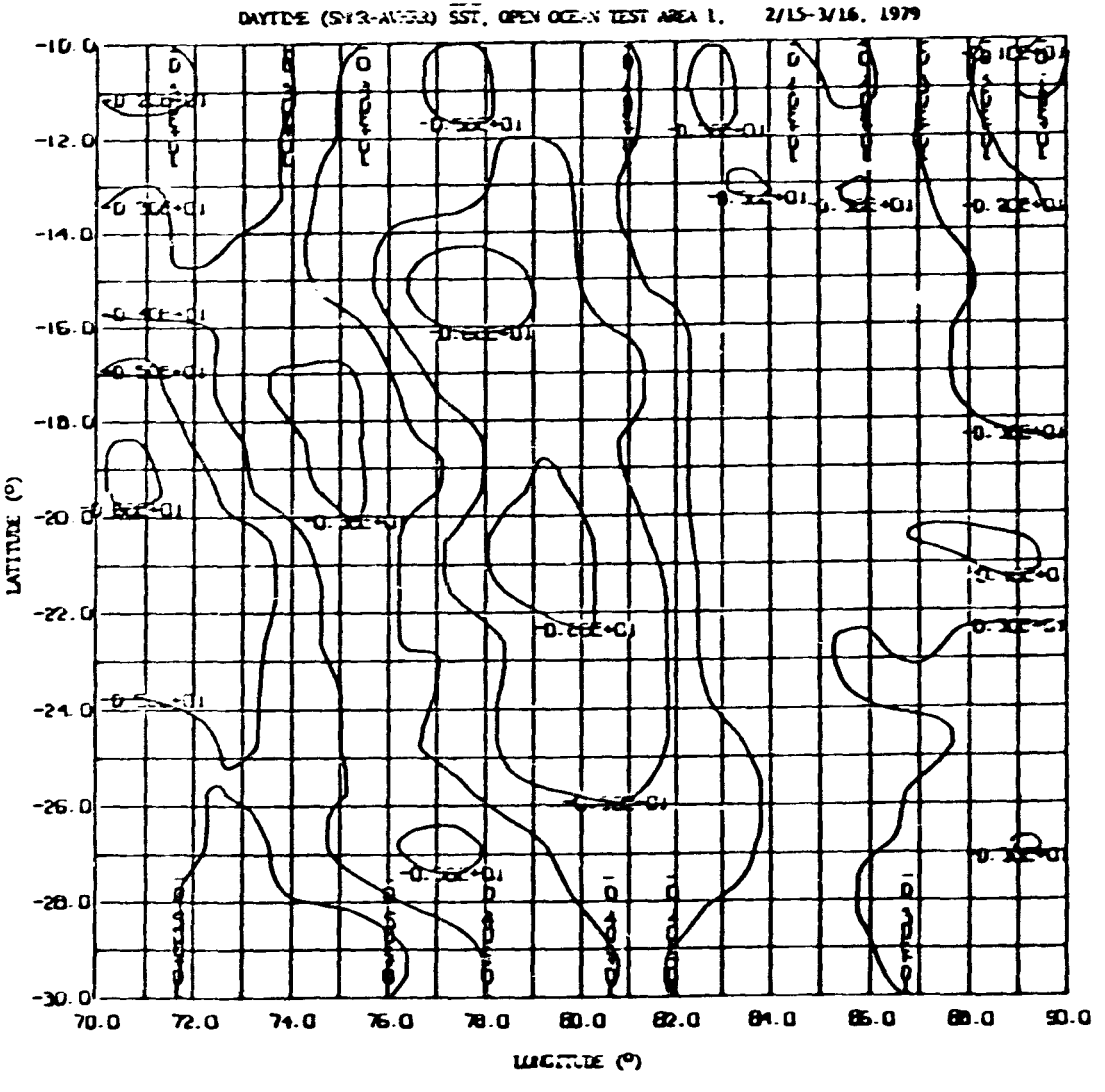
DAYTIME (SYM-AVHRR) SST, OPEN OCEAN TEST AREA 1. 2/15-3/16, 1979
-10.0
-12.0
-14.0
-16.0
-18.0
-20.0
-22.0
-24.0
-26.0
-28.0
-30.0
LATITUDE (°)
70.0
72.0
74.0
76.0
78.0
80.0
82.0
84.0
86.0
88.0
90.0
LONGITUDE (°)

FIGURE 3.2-4

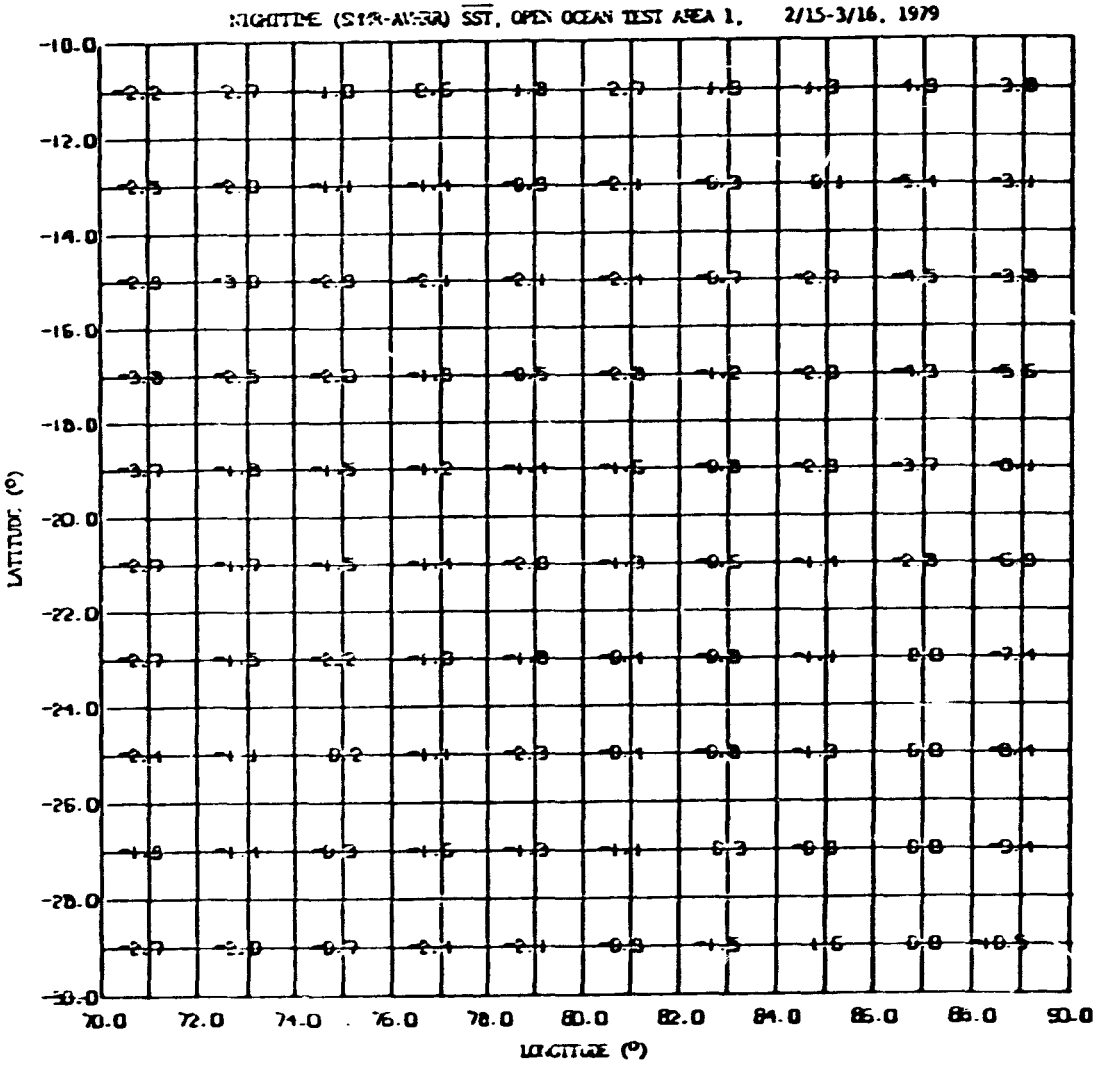
NIGHTTIME (STRATIFIED) SST, OPEN OCEAN TEST AREA 1, 2/15-3/16, 1979
-10.0
-12.0
-14.0
-16.0
-18.0
-20.0
-22.0
-24.0
-26.0
-28.0
-30.0
LATITUDE (°)
70.0
72.0
74.0
76.0
78.0
80.0
82.0
84.0
86.0
88.0
90.0
LONGITUDE (°)

FIGURE 3.2-5

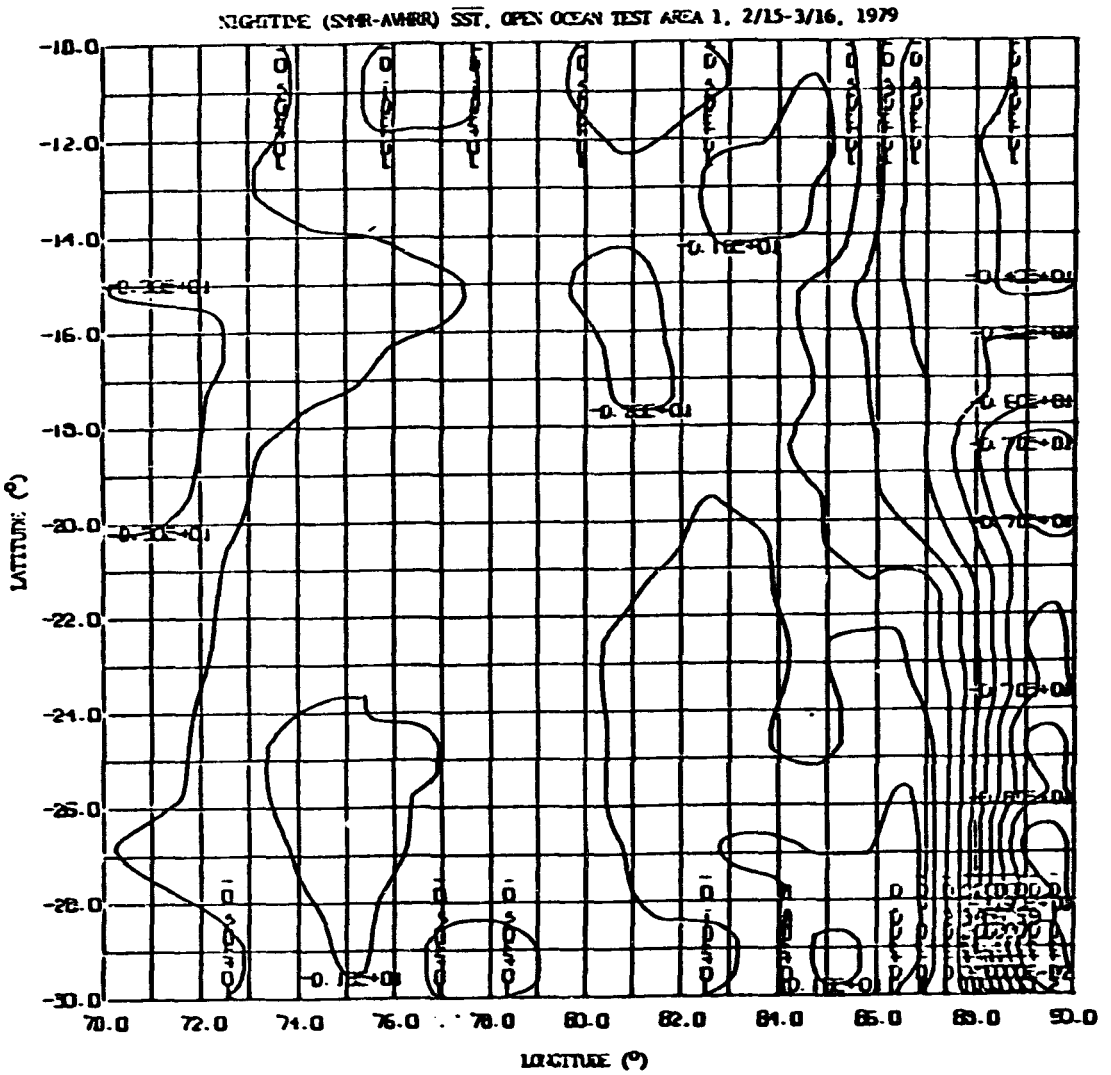
NIGHTTIME (SMMR-AMHRR) SST, OPEN OCEAN TEST AREA 1, 2/15-3/16, 1979
-10.0
-12.0
-14.0
-16.0
-18.0
-20.0
-22.0
-24.0
-26.0
-28.0
-30.0
LATITUDE (°)
70.0
72.0
74.0
76.0
78.0
80.0
82.0
84.0
86.0
88.0
90.0
LONGITUDE (°)

It is noticed that the SMMR SST retrievals are always smaller than the AVHRR retrievals and that there is a tendency for SMMR daytime and nighttime retrievals to differ by more than 1°C; the exceptions are in test areas 2 and 5, northern hemisphere mid-latitude regions, where the daytime and nighttime differences are less than 0.9°C. A rather curious observation appears when Table 3.2-II is looked at; both AVHRR and SMMR SST distributions are wider in the mid-latitudes of the northern and southern hemispheres implying larger variations in SST in each test area during this time period. More in depth investigation of this will have to be done to determine whether or not we are seeing the effects of real physics.

A comparison of Table 3.2-I with Table 3.2-II shows that for the open ocean test areas the SMMR day/night SST differences are consistently smaller than the SST differences in ocean areas within several hundred kilometers of land. For example, look at the SMMR statistics around buoys 17 and 20 which are farthest away from land. At 17 the SMMR SST day/night difference is 5.0°C; at 20 this SST difference is much smaller but the width of the two distributions differ by a factor of about 3.5. Such differences never appear in the open ocean areas as shown in Table 3.2-II.

Another region chosen to make comparison of SMMR and AVHRR is off the east coast of the United States defined by 25°N-45°N latitude and 56°W-80°W longitude. This is shown in the cross-hatched region adjoining the ocean test area 5 of Figure 3.2-1. The statistics were computed in the same way as for the ocean test areas. The comparison of SMMR and AVHRR was made a function of distance from land in 2° latitude intervals. The results are shown in Figures 3.2-6 - 3.2-10.

Defining the parameter

$$\delta = SST_{SMMR} - SST_{AVHRR}$$

it is seen that in the daytime, $\delta < 0$ at all latitude bands.

The strong negative bias possessed by the daytime SMMR retrievals ranges from -2.2°C to -5°C with the average being -3.7° C. If the respective bias is removed from each latitude band it is seen that the SMMR retrievals never differ by more than $\pm$1°C from the AVHRR retrieval. The bias is plotted as a function of latitude and shown in Figure 3.2-11.

TABLE 3.2-III

BUOY	AVHRR SST	AVHRR σ	SMMR DAY SST	SMMR DAY σ	SMMR NIGHT SST	SMMR NIGHT σ
1	19.8	0.9	19.5	0.9	24.7	1.1
2	21.8	1.3	21.7	1.2	26.4	2.3
12	11.5	3.8	9.1	2.3	14.8	3.4
13	14.0	2.2	11.9	1.4	18.7	2.7
14	4.0	1.3			10.2	1.2
16	11.4	0.4	15.4	0.4	14.6	5.4
17	3.4	0.4	8.7	1.3	4.1	0.4
18	7.0	0.5	15.9	0.9	10.0	3.7
19	9.3	0.5	14.2	1.1	16.7	3.8
20	11.9	0.6	12.5	0.9	12.5	1.6

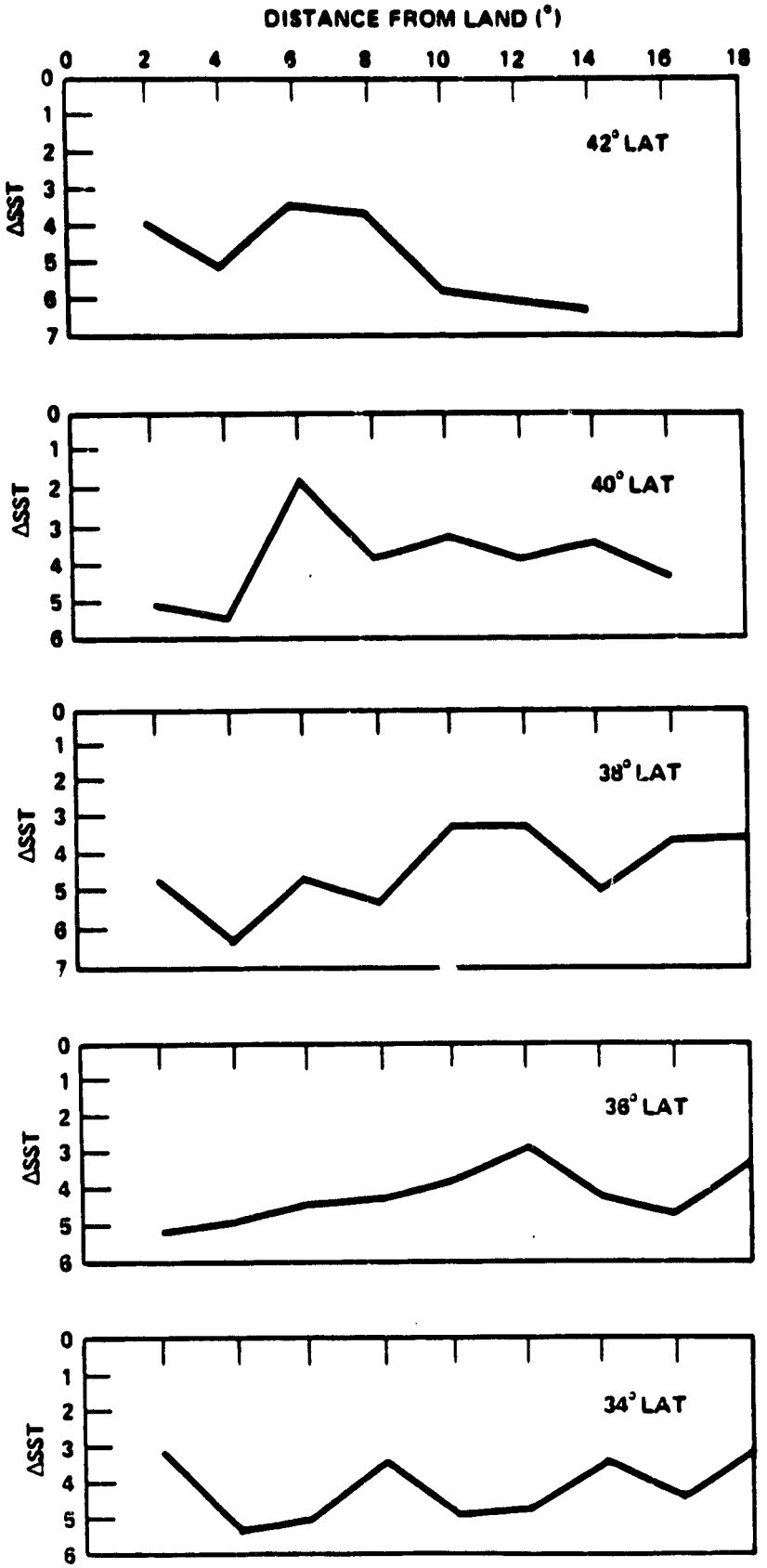

FIGURE 3.2-6 (SMMR-AVHRR) Day $\overline{SST}$

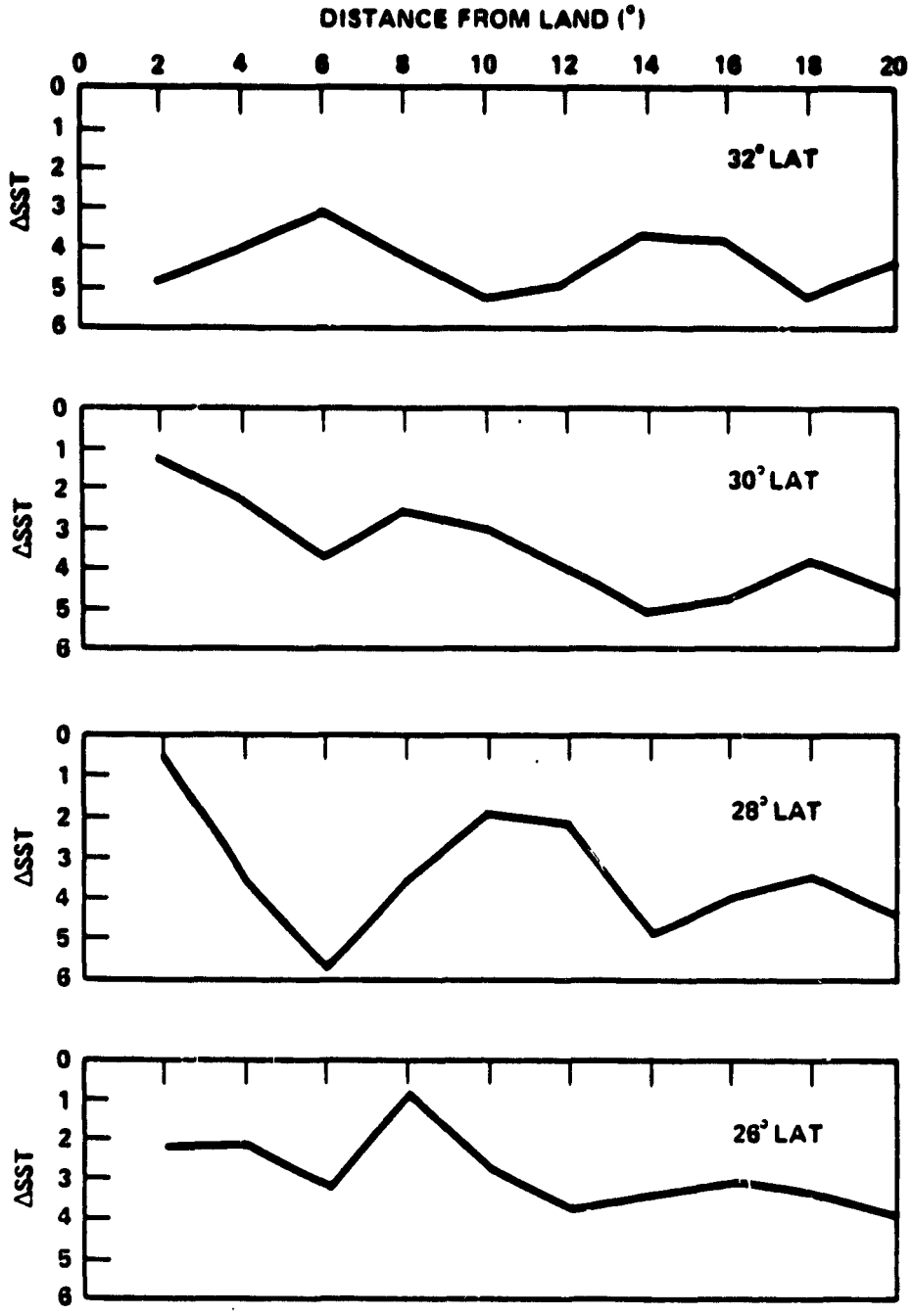

FIGURE 3.2-7 (SMMR-AVHRR) Day $\overline{SST}$

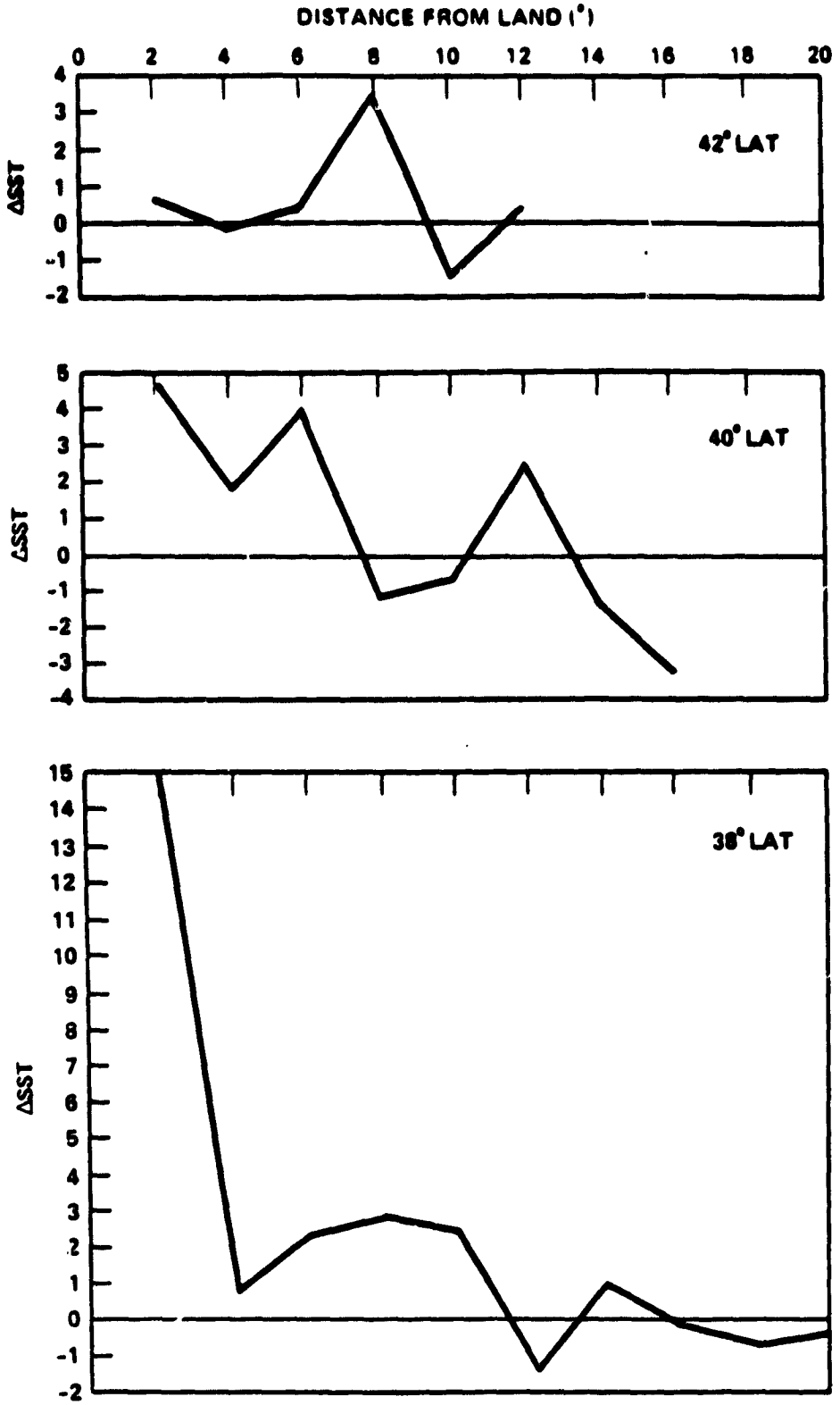

FIGURE 3.2-8 (SMMR-AVHRR) Night $\overline{SST}$

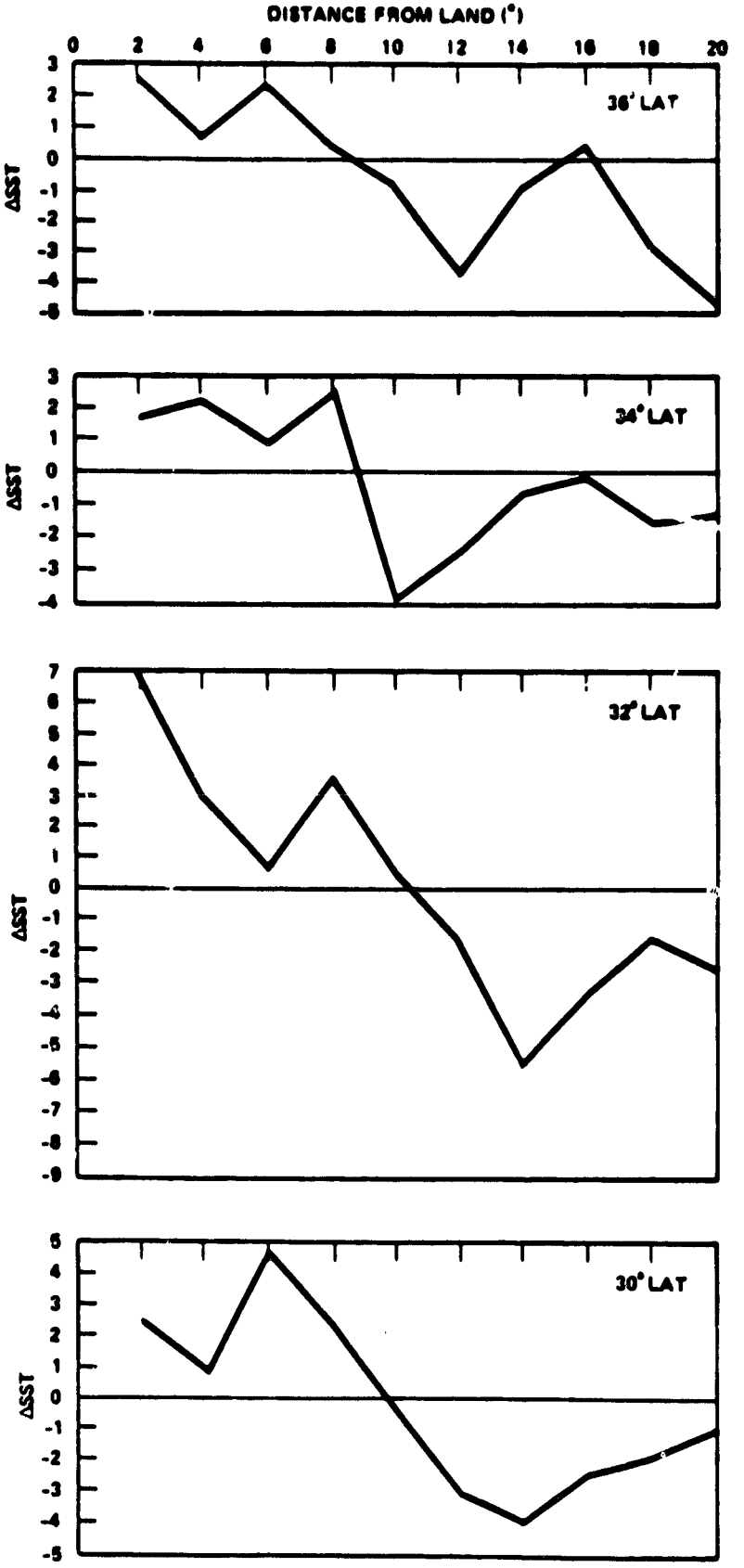

FIGURE 3.2-9 (SMMR-AVHRR) Night $\overline{SST}$

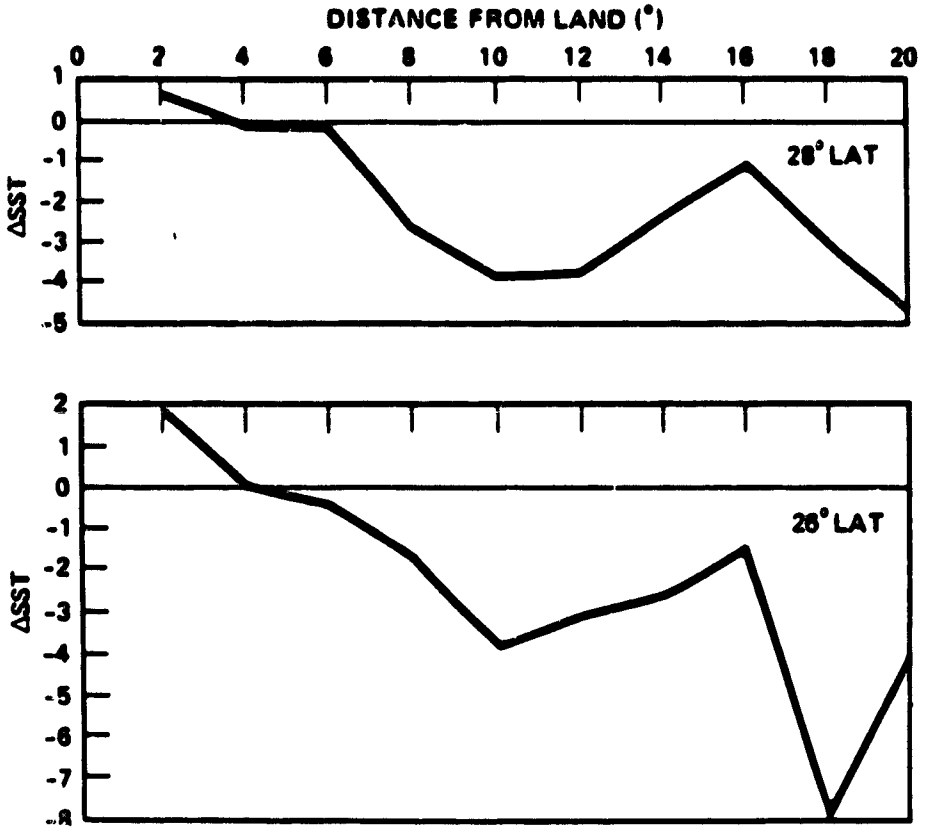

FIGURE 3.2-10 (SMMR-AVHRR) Night $\overline{SST}$

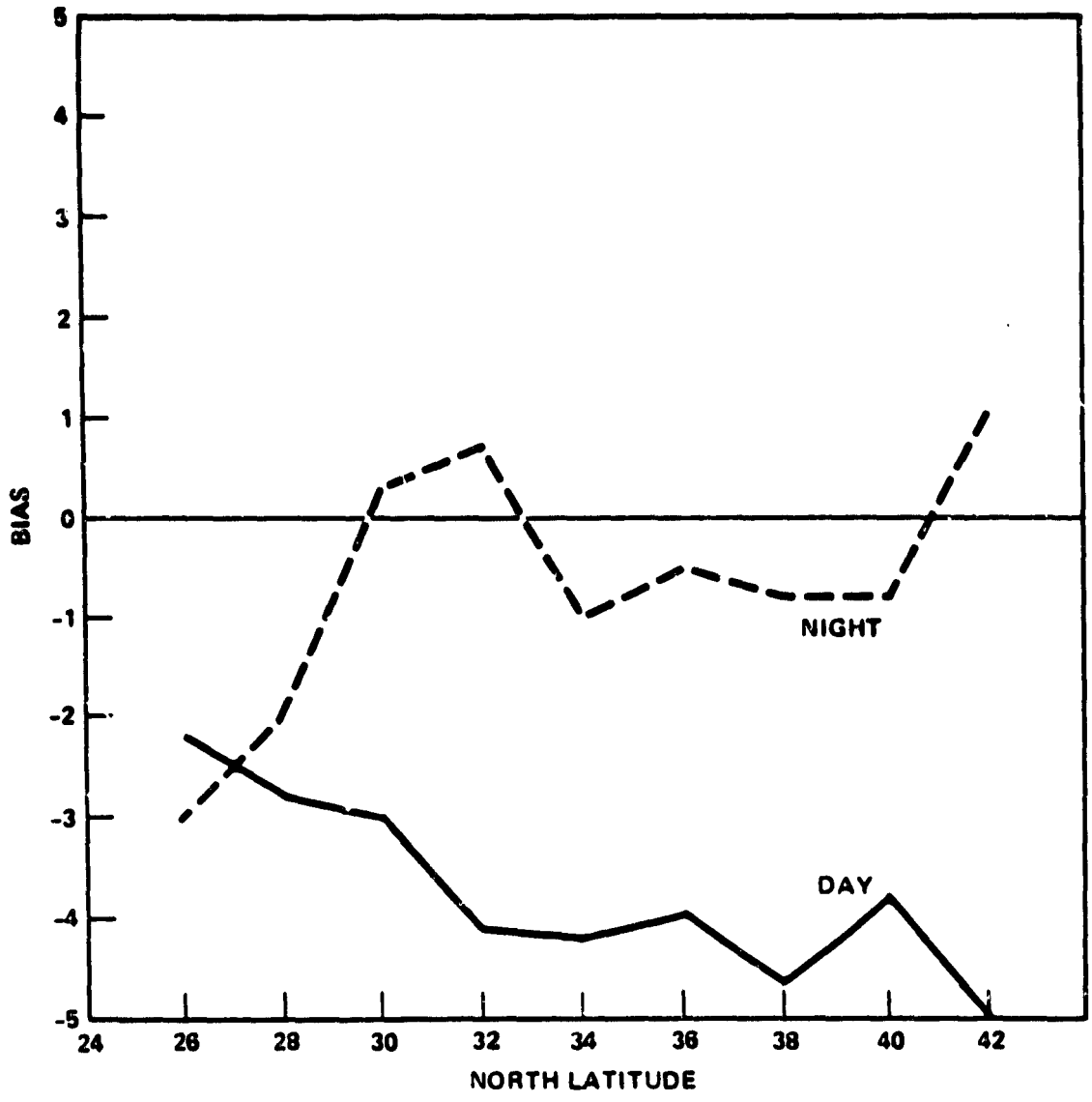

FIGURE 3.2-11 Bias Along the East Coast U.S.

The east coast nighttime results are vastly different. The values of are always positive out to roughly 8°-10° from land. The transition from positive to negative values of δ occurs over a distance of 6° to 10° from land. There is no strong negative bias with the nighttime results; in fact our computations show that the biases range from +1°C to -3°C with the average bias being -0.37°C. These computations assume that the very large difference shown at 38°N latitude is an anomaly and consequently has been neglected. Again unlike the daytime results, the SMMR retrievals at night show a much wider distribution about the AVHRR with peak-to-peak variations being as great as about 3.8°C. So even though the nighttime results have an average bias which is almost 9 times smaller magnitude than the daytime results, the nighttime results show a maximum distribution about the AVHRR SST of about 4 times greater than that shown by the daytime results.

Since the results along the east coast were so different, it was decided to test other coastal regions to see if the same behavior is observed. The results shown in Figures 3.2-11 through 3.2-23 cover the west coast of the United States and the west coast of Australia.

The results off of the west coast of the United States shows much different behavior then the east coast results. The daytime results shows SMMR retrievals greater than AVHRR out to about 17° from the coast along some latitude bands. Another curious behavior of the daytime data is the tendency of the zero crossing to decrease with latitude band until the 43° band is reached at which point the zero crossing remains in the 7°-8° interval. No physical reason for this has emerged from our analysis. Separation of the daytime results according to $\delta > 0$ and $\delta < 0$ shows some additional structure not present in the east coast results. The peak-to-peak variation when $\delta > 0$ ranges from 1° to 2.5°; when $\delta < 0$ the peak-to-peak variation ranges from about 1.0° to 2.0° with the strong tendency to become larger with decreasing latitude band. The daytime results show biases ranging from -0.7°C to +2.8°C with an average bias of +0.27°C.

The nighttime results off of the west coast of the United States is again quite different from the daytime data. The zero crossings are consistently in the 4°-6° interval except for the 31° and 33° latitude bands. When $\delta < 0$, the peak-to-peak variation ranges from less than 1°C to 3°C; when $\delta < 0$ this variation ranges from about 1.5°C to 3°C. The biases which were computed range from -2.6°C to +0.7°C with the average bias computed to be -1.0°C. The biases off of the west coast of the United States are plotted as a function of latitude in Figure 20.

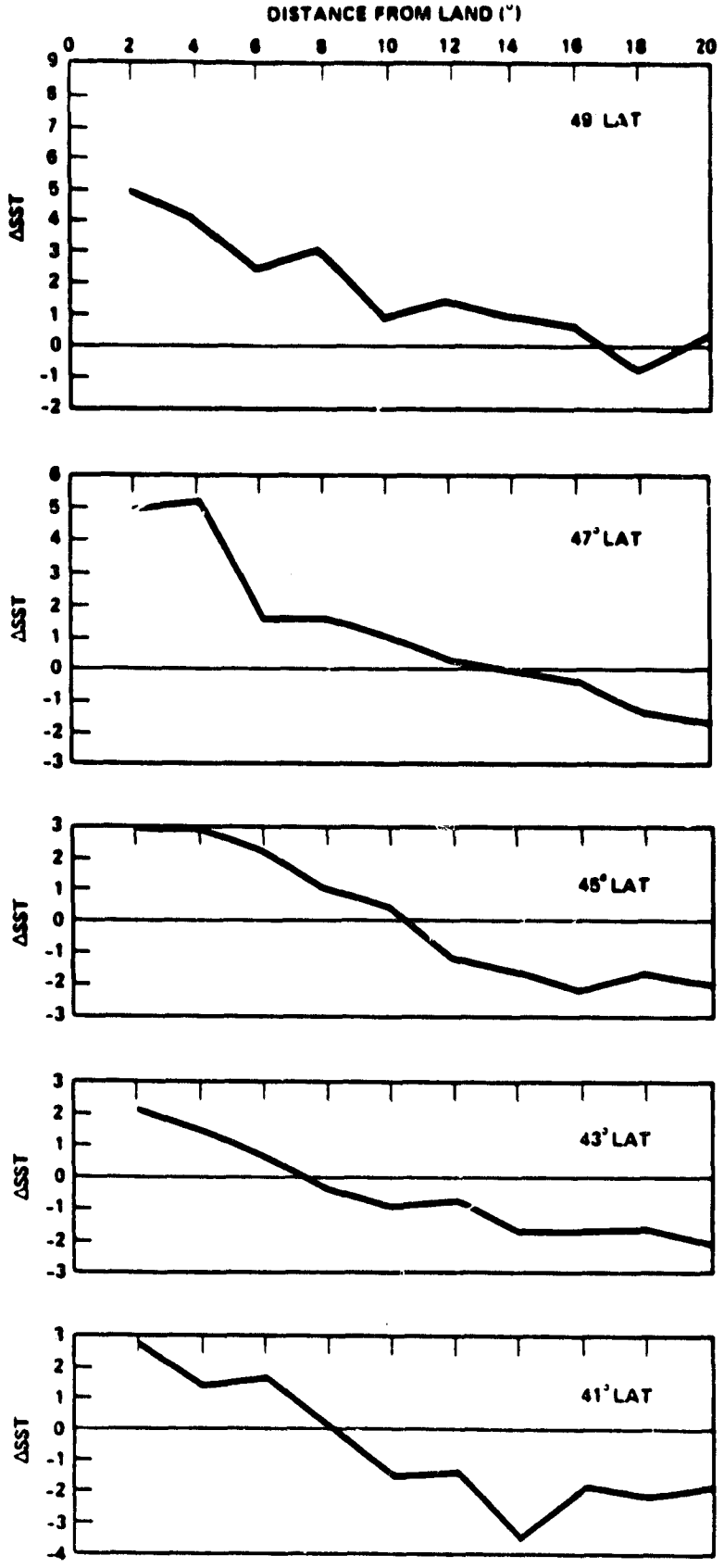

FIGURE 3.2-12 (SMMR-AVHRR) Day $\overline{SST}$

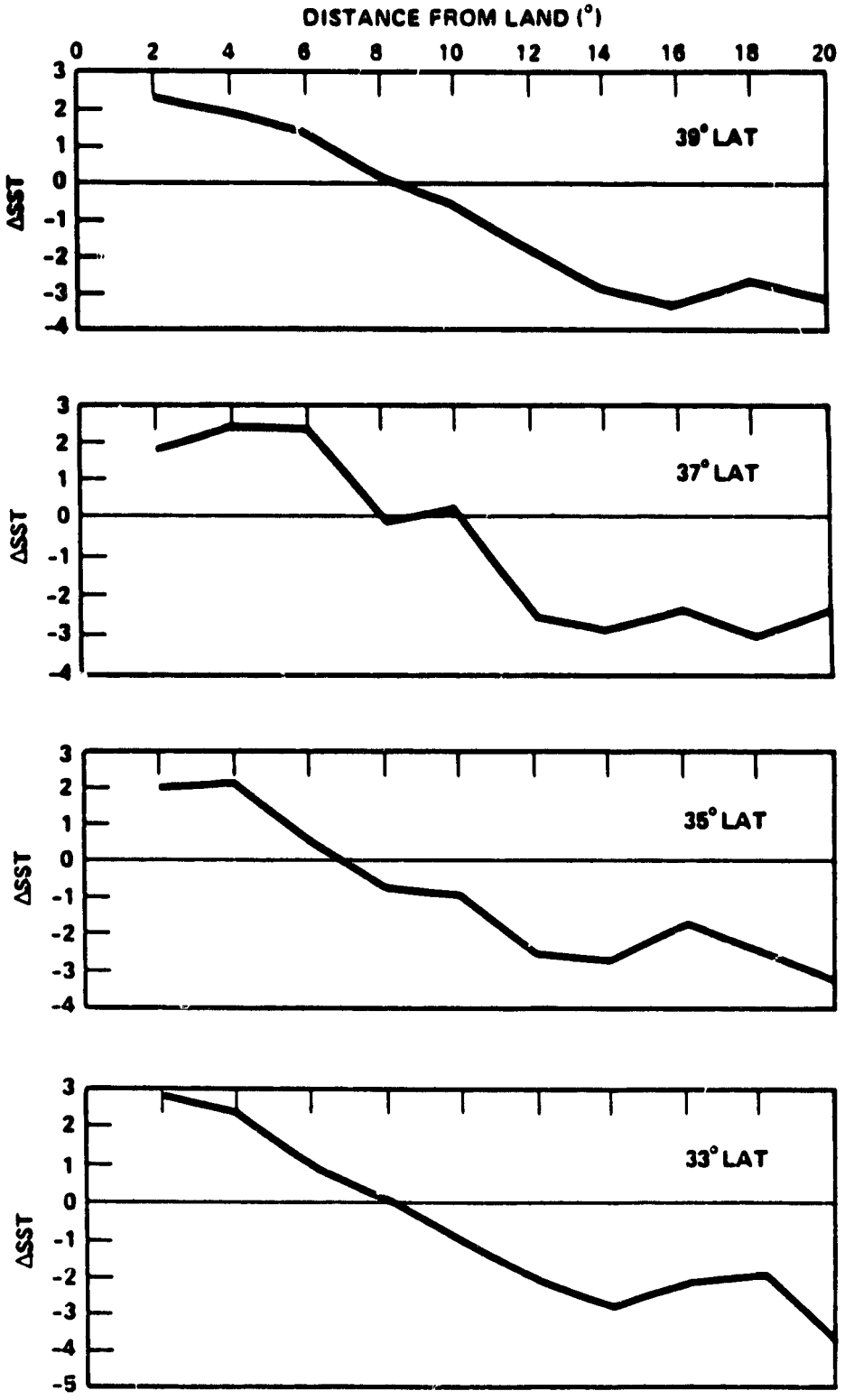

FIGURE 3.2-13 (SMMR-AVHRR) Day $\overline{SST}$

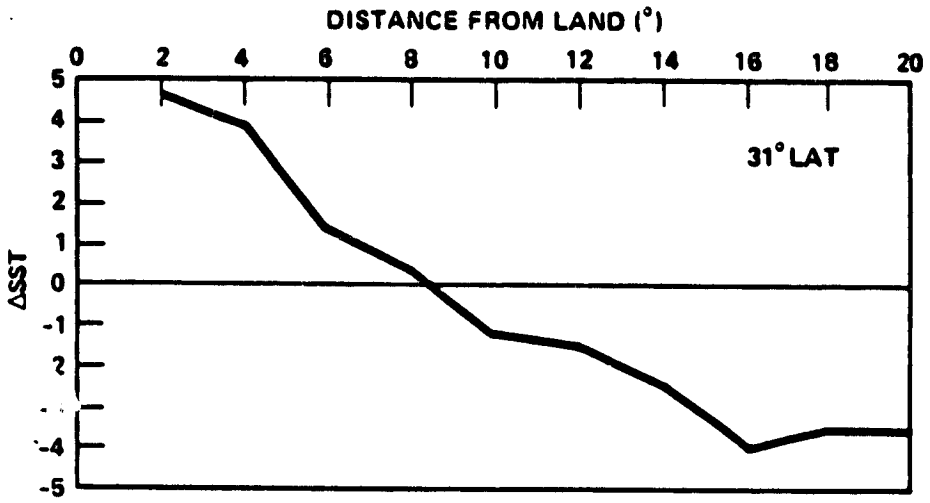

FIGURE 3.2-14 (SMMR-AVHRR) Day $\overline{SST}$

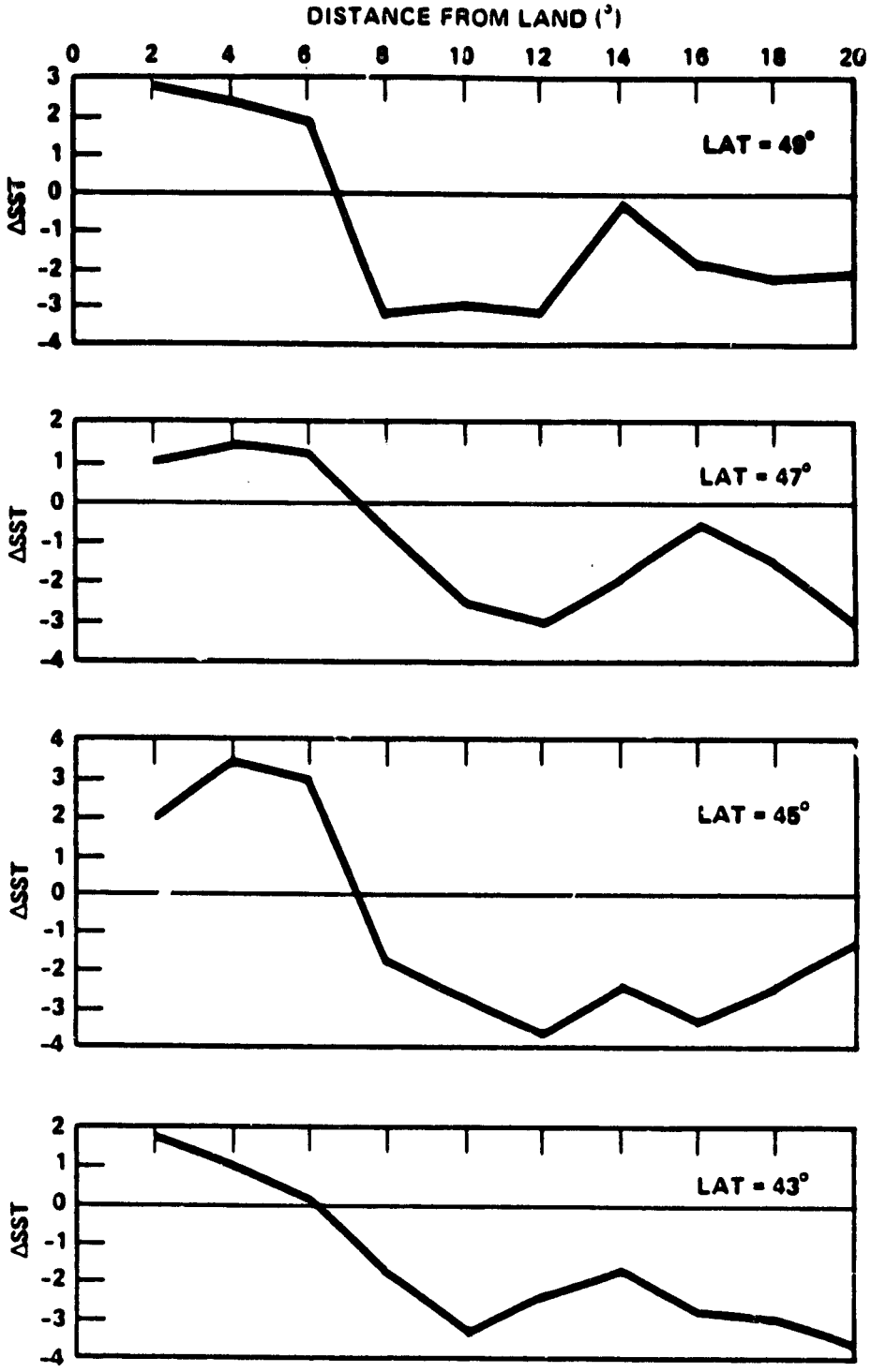

FIGURE 3.2-15 (SMMR-AVHRR) Night $\overline{SST}$

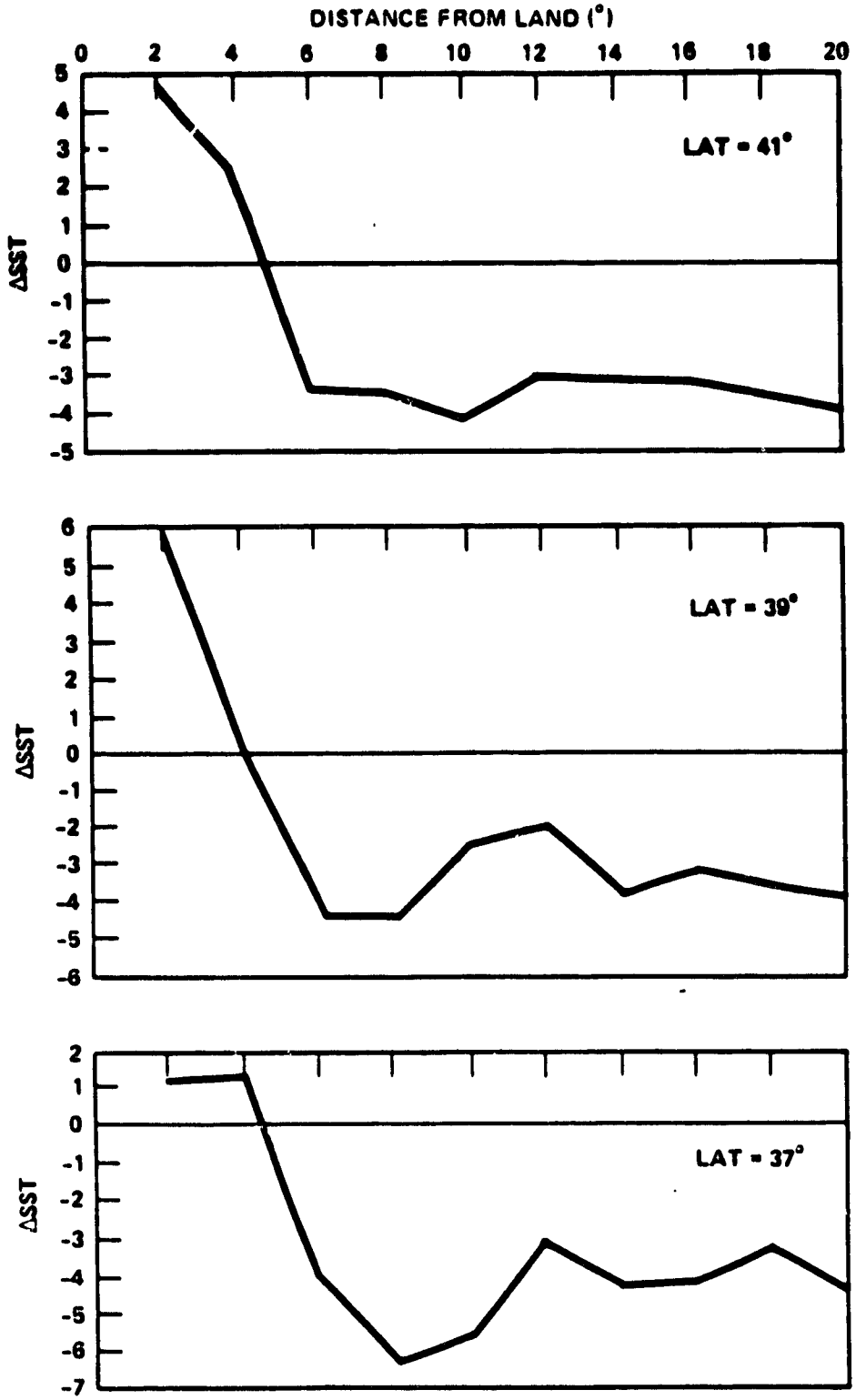

FIGURE 3.2-16 (SMMR-AVHRR) Night $\overline{SST}$

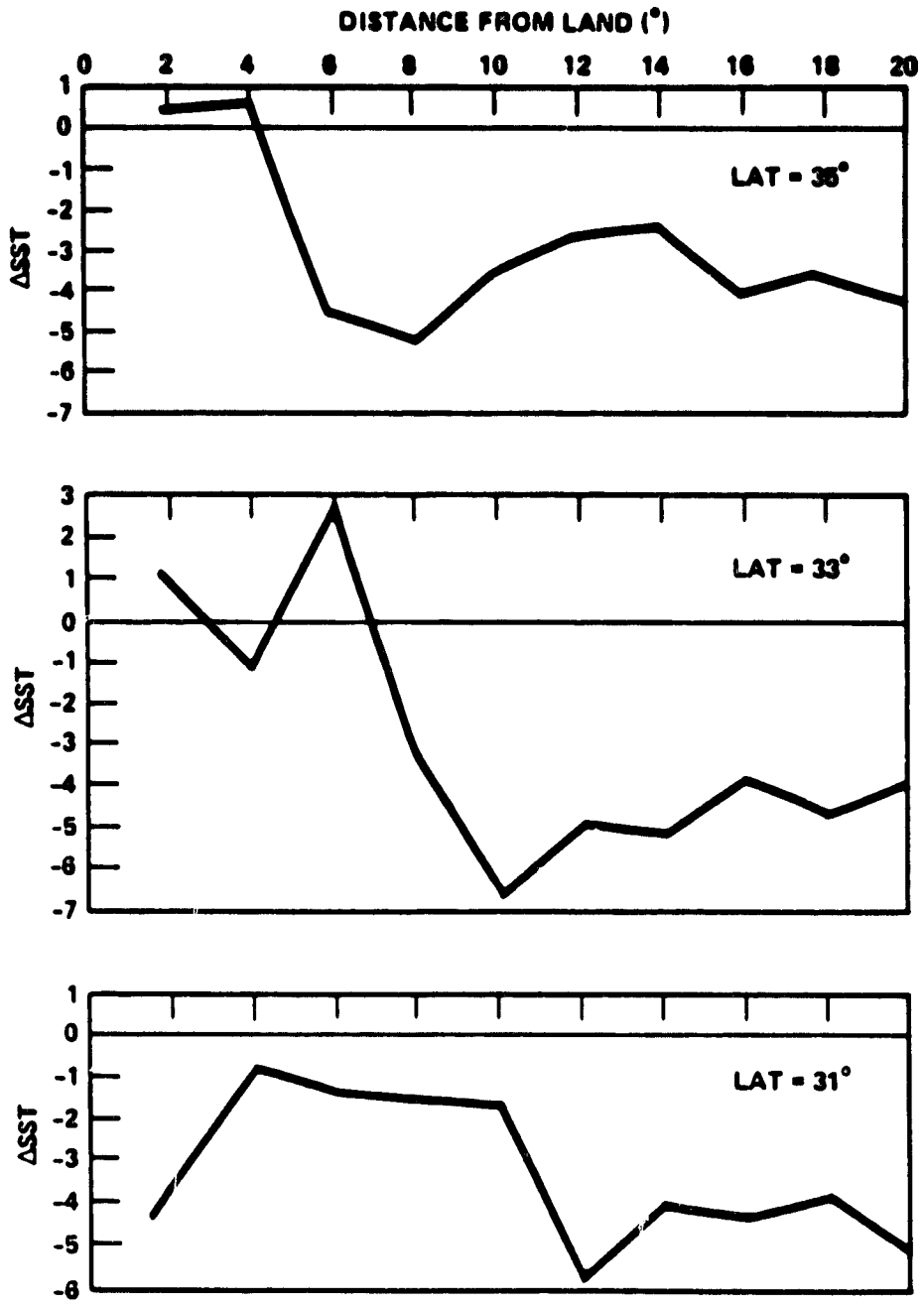

FIGURE 3.2-17 (SMMR-AVHRR) Night $\overline{SST}$

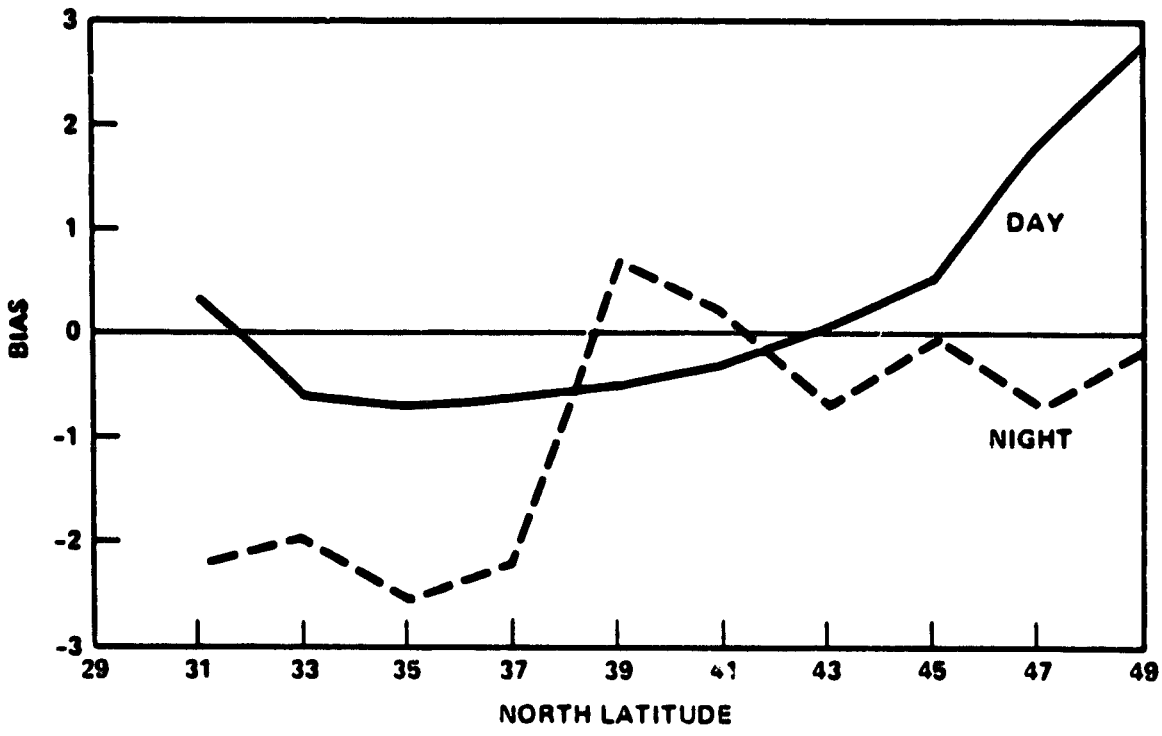

FIGURE 3.2-18 Bias Along the West Coast U.S.

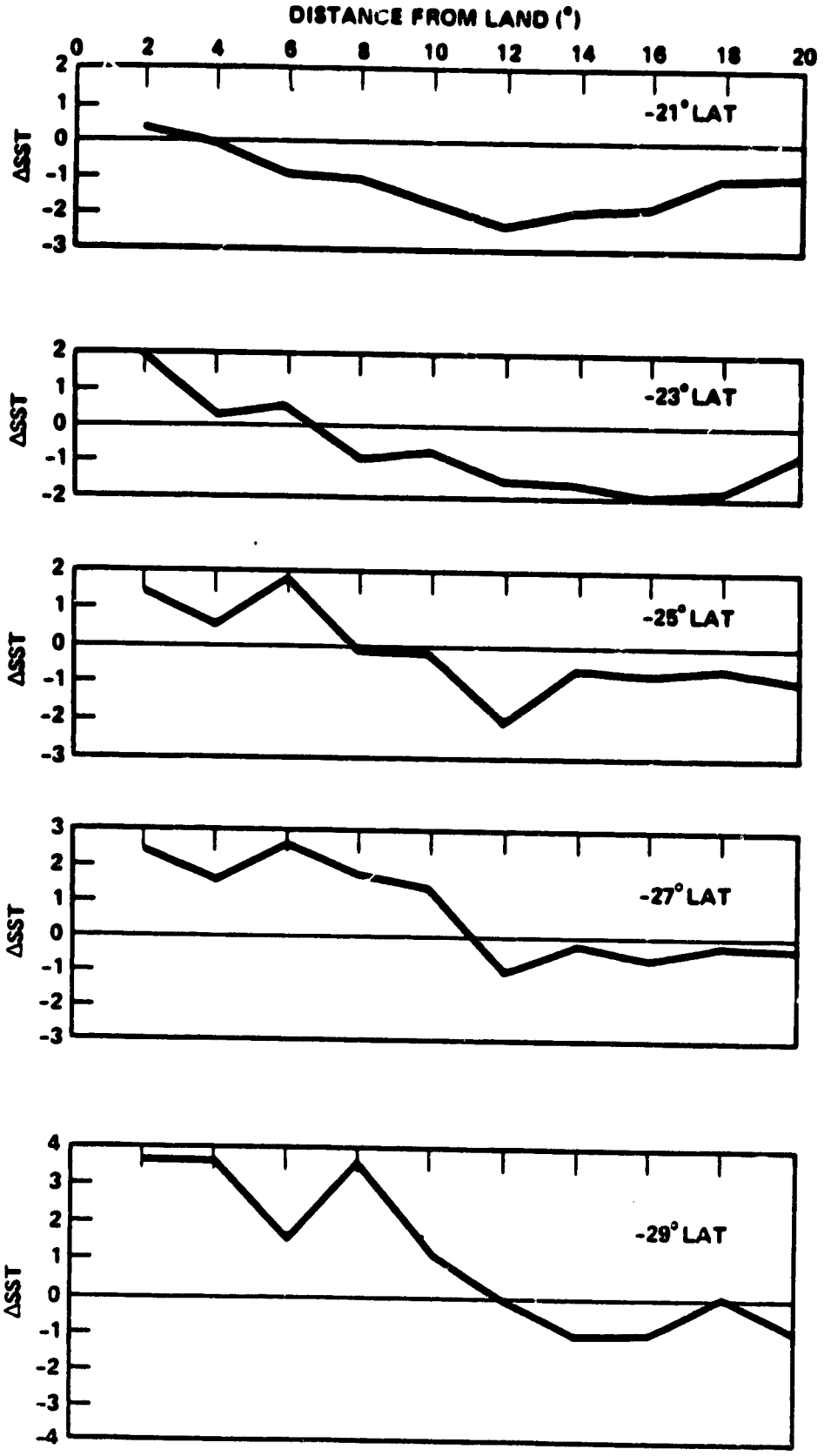

FIGURE 3.2-19 (SMMR-AVHRR) Day $\overline{SST}$

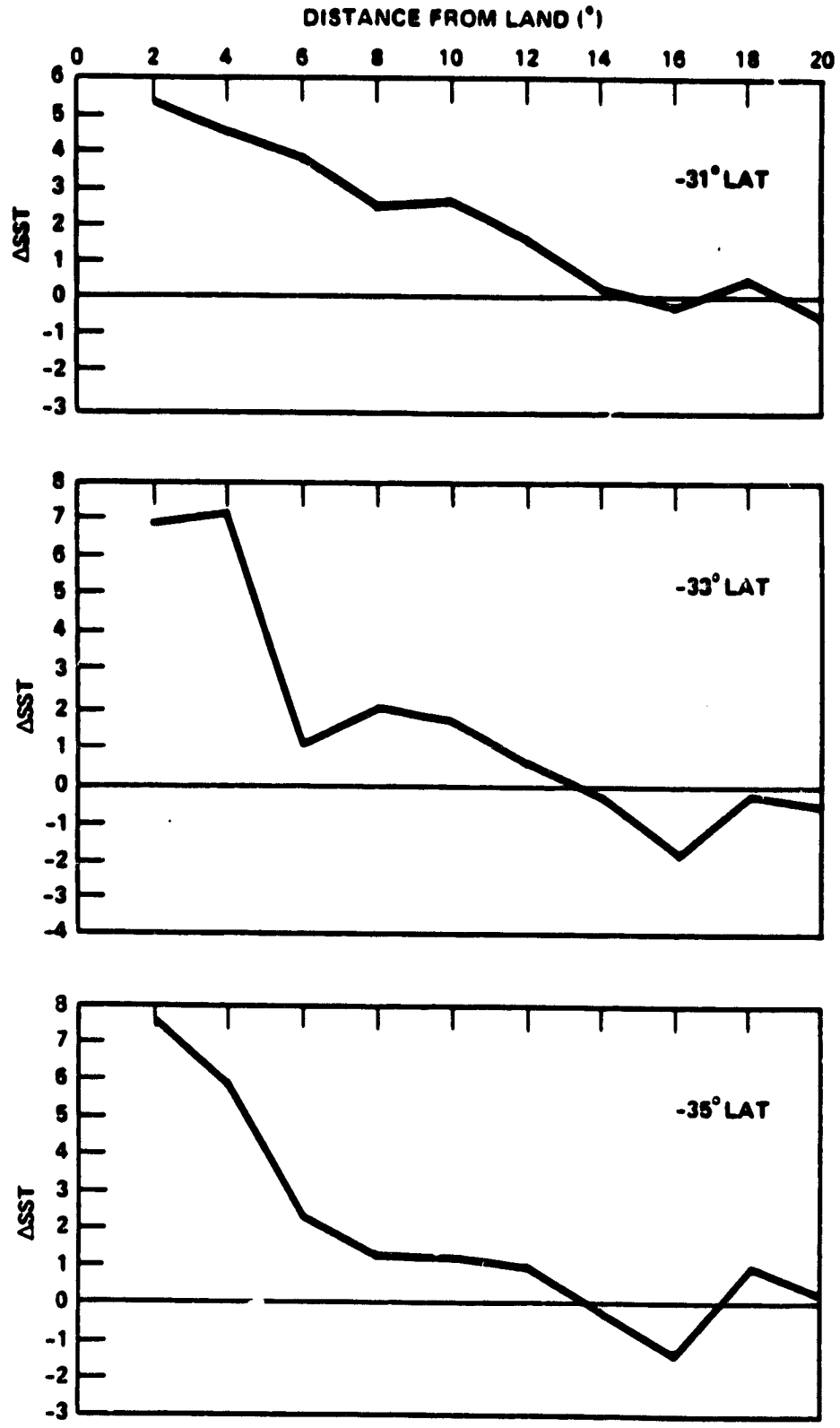

FIGURE 3.2-20 (SMMR-AVHRR) Day $\overline{SST}$

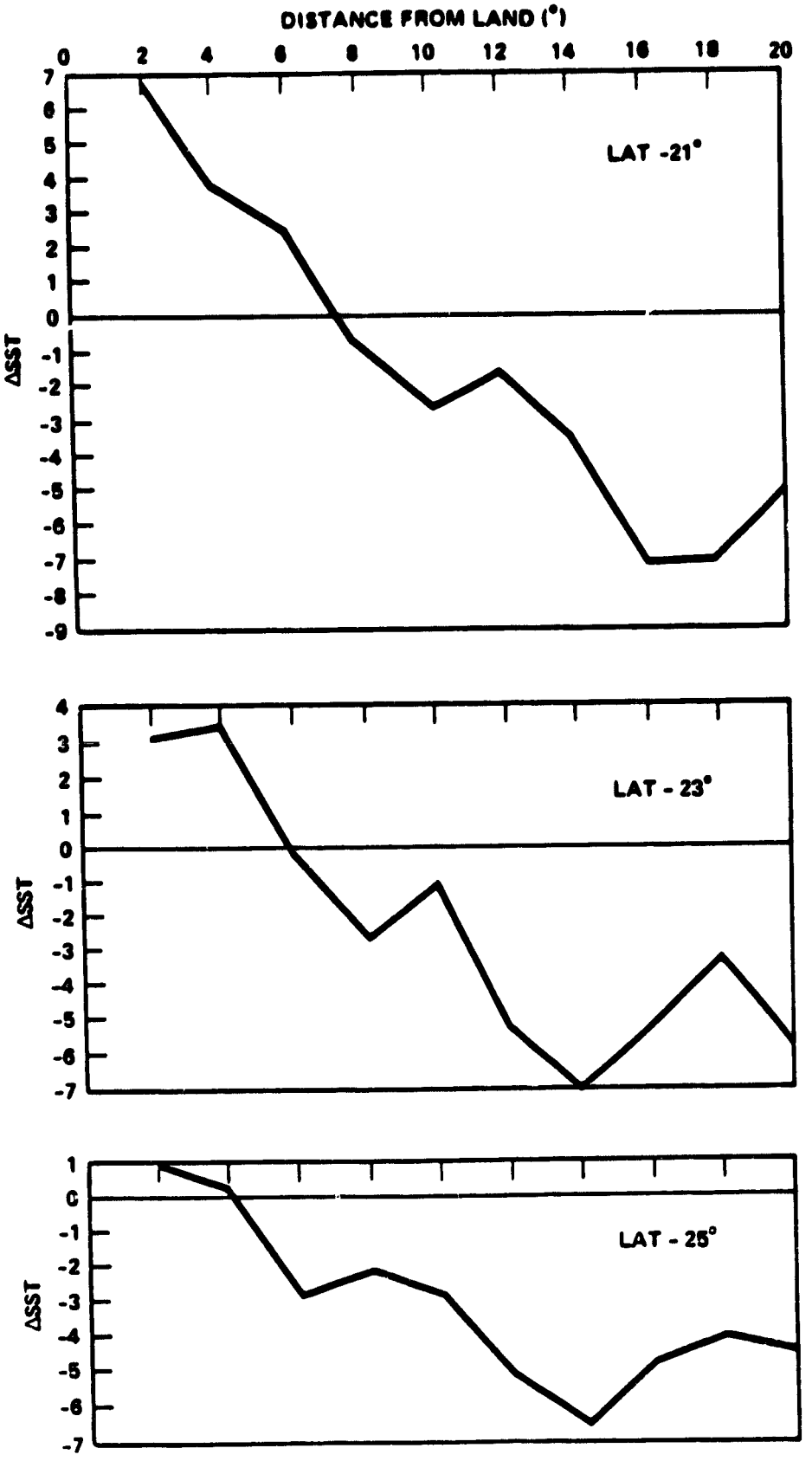

FIGURE 3.2-21(SMMR-AVHRR) Night $\overline{SST}$

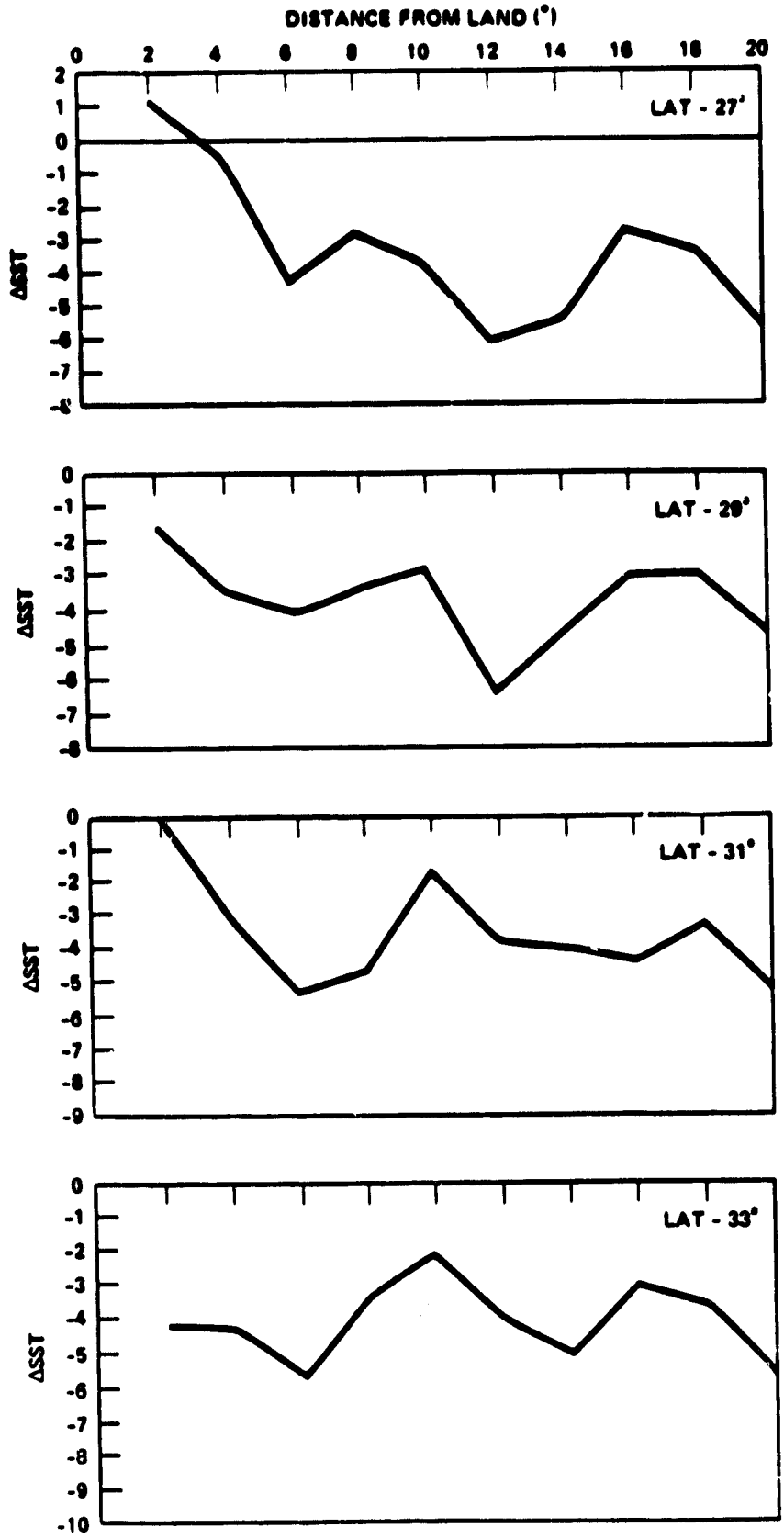

FIGURE 3.2-22(SMMR-AVHRR) Night $\overline{SST}$

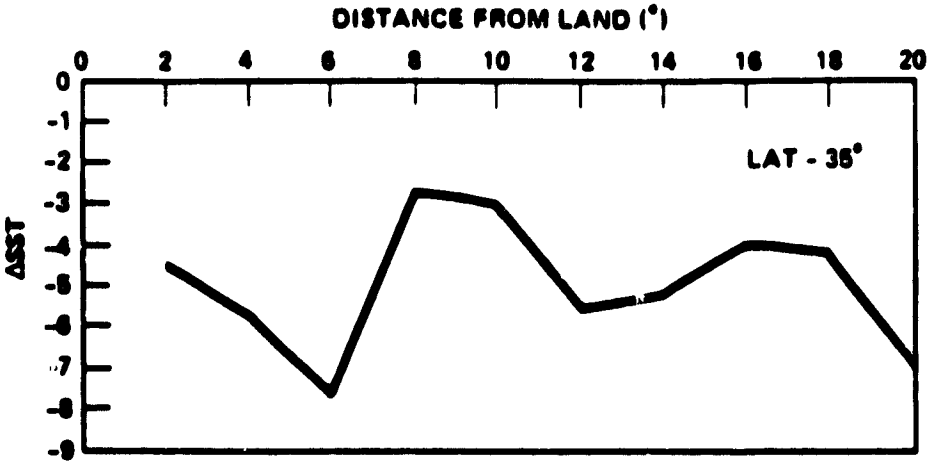

Figure 25. (SMMR-AVHRR) Night $\overline{SST}$

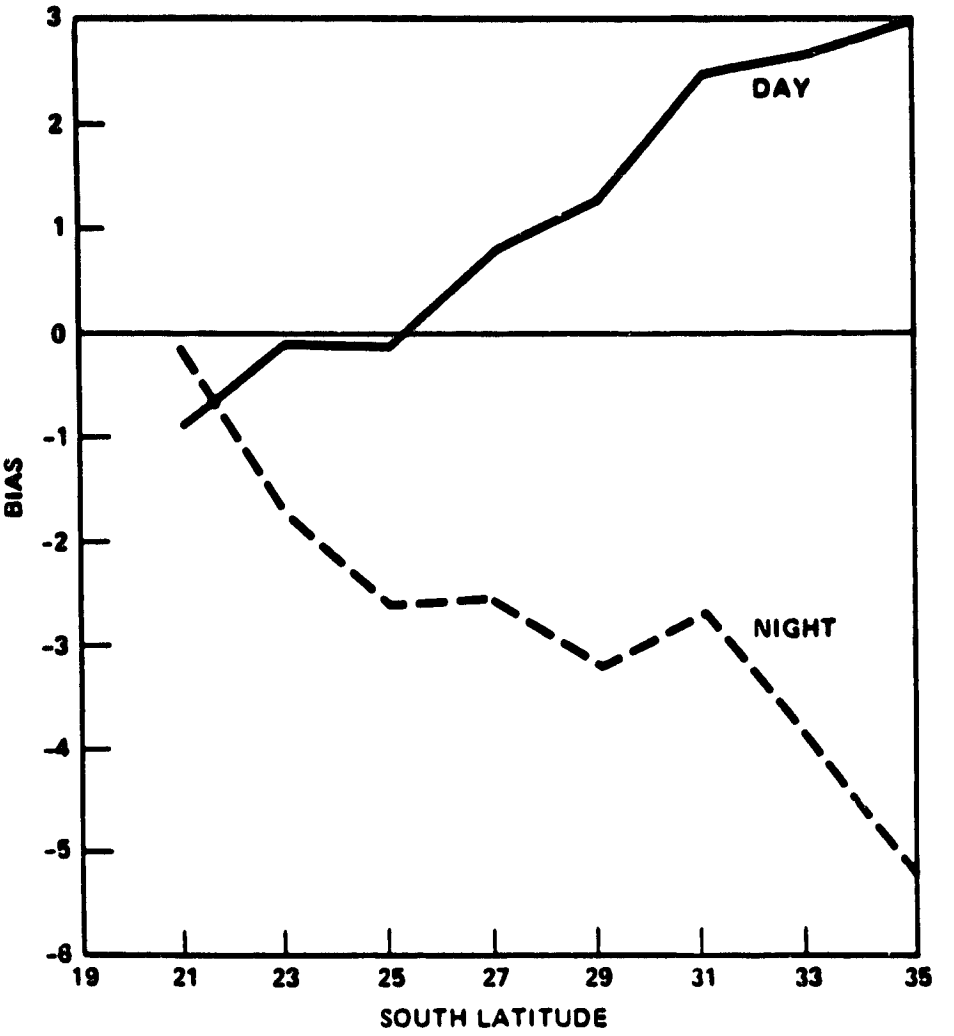

FIGURE 3.2-23 Bias Along the West Coast Australia

The results off of the west coast of Australia show still another kind of behavior. The daytime results at 21°S are rather flat and tend to show progressively larger peak-to-peak variations as latitude increases to the south. Moreover, the zero crossing also tends to increase with increasing southern latitude. The computed biases range from -0.9°C to +3.0°C with the average bias being +1.0°C.

The nighttime results show rather large variations for both $\delta<0$ and $\delta>0$ at 21°S; there is a tendency for the SMMR retrievals to get smaller as southern latitude is increased. The computed biases range from -0.15°C to -5.2°C with the average bias computed to be -2.8°C. Omitting the 21°S latitude band, it is seen that the maximum peak-to-peak variation is $\pm$5°C and this occurs at 23°S latitude.

In this case, in the southern hemisphere, the average bias of the daytime data is about 6 times smaller in magnitude than the nighttime result. The nighttime results however show a tendency to be more widely scattered about the AVHRR over all latitude bands even though the peak-to-peak maximum is about $\pm$5° C for both daytime and nighttime results.

Having computed the biases in the large ocean areas 2 and 5, shown in Figure 3.2-1, it was felt it would be of interest to take these biases out of the SMMR retrievals around each of the appropriate buoys. The bias computed in region 5 was applied to buoys 1 and 2 and buoys 12 and 14; the bias computed in region 2 was applied to buoys 16 thru 20. The results are presented in Table 3.2-III and support the hypothesis that SMMR is affected by radio frequency interference, or some other effect occuring when the SMMR FOV's are near the land-ocean interface. For example, when the bias is applied to SMMR nighttime retrievals around buoys 1 and 2, the retrievals become significantly worse; whereas the daytime retrievals agree almost perfectly with the AVHRR retrievals. Similar comments can be made concerning buoys 12 thru 14. The nighttime retirevals are affected because the SMMR ground track tends to be parallel to the eastern coastline whereas the daytime passes make an acute angle with the coastline. For the same reason, the nighttime retrievals at buoys 16 thru 20 tend to be in much better agreement with the AVHRR because along the western coastline it is the nighttime pass which makes an acute angle with the coastline. The exceptions to this argument are at buoys 19 and 20. Buoy 20, it is recalled, lies well off the coast; more than 12° from land where RFI effects are expected to be small. Buoy 19 however is an anomalous case and will require further study.

A preliminary comparison between the SMMR and AVHRR SST retrievals using the new SMMR CELL tapes was carried out for an open ocean region in the equatorial Pacific. AVHRR and SMMR SST's were binned into 2^{o} x 2^{o} latitude-longitude blocks in the ocean region 0^{o} to 20^{o}N and 180^{o}-150^{o}W for the February 15 through March 16, 1979 time period. The SMMR data was divided into day and night observations and compared with the AVHRR SST's and statistics for the month were computed. This test area is near open ocean area 3 above where comparison were made between the AVHRR SST's and those from the original SMMR CELL tapes. Table 3.2-IV shows the results of the SMMR AVHRR SST comparison in this area. While the absolute difference between the SMMR and AVHRR SST's is expected to be different from the data in area 3 above because of the new calibration data used to produce the SMMR CELL tape and because the geographical area is somewhat different, it can be from the standard deviation (σ) of the SMMR-AVHRR SST's that the daytime differences seems to be noisier than the previous comparison and the nighttime comparison quieter.

TABLE 3.2-IV

LATITUDE	LONGITUDE	AVHRR SST				SMMR SST			(SMMR-AVHRR)SST		
		SST(°C)	σ(°C)	POP		SST(°C)	σ(°C)	POP	SSI(°C)	σ(°C)	POP
0°N-20°N	180°W-150°W	25.4	2.3	144	DAY	19.9	1.8	149	-5.7	1.5	143
					NIGHT	20.7	1.2	149	-4.9	0.7	143

4.0 CONCLUSIONS

4.1 SMMR Analysis

Preliminary NIMBUS-7 Scanning Multichannel Microwave Radiometer (SMMR) brightness temperature measurements for the November-December 1978 and February-March 1979 time periods have been analyzed and evaluated. In addition, the geophysical parameters (primarily sea surface temperature) retrieved using the SMMR brightness temperatures and current algorithms have been evaluated and compared with ocean measurements from independent sources.

The primary conclusions which can be drawn from this study are:

- The brightness temperatures measured by the SMMR for the October-November 1978 and February-March 1979 time periods were found to be generally close to the T_b's expected for the specified frequency and SMMR field of view. The effect of polarization mixing between the two polarization modes was observed in the T_b's as a cross track bias in the T_b's. Empirical correction factors were computed based on the T_b observations for two weeks of October-November 1978 data. When these correction factors were applied to the T_b observations, it was found that they eliminated the cross track bias almost completely for the T_b data for the time period from which they were computed, but were less effective in eliminating the bias for other time periods. In all cases however, the T_b's with the empirical corrections produced a smaller cross track bias then the uncorrected data.
- The comparison between SMMR retrieved sea surface temperatures and surface truth observations from buoys, and operational SST retrievals from the infrared sensors on the TIROS-N spacecraft (AVHRR) show that the SMMR SST retrievals have a warm bias compared with the buoy SST's, and are considerably noisier compared with the AVHRR data. In open ocean comparisons between the AVHRR and SMMR SST's the SMMR data has a warm bias compared with the AVHRR data and again the SMMR SST retrievals are considerably more noisy than the AVHRR retrievals. In addition, near land ocean boundaries the comparison of

SMMR and AVHRR SST's shows the influence of a bias due to the spacecraft coastline relative geometry. This bias may be due to antenna sidelobe effects, coastal radio frequency interference or a combination of these two factors.

The relatively small amount of SMMR T_b data (42 days over 9½ weeks of the Autumn and Winter) makes it hard to draw any firm conclusions concerning the time variations of the SMMR retrievals. The data which was used for comparison was also limited. The buoys were located near the coast where sidelobe and RFI effects make the SMMR retrievals unreliable. The necessity for eliminating duplicate SST observations present in the AVHRR data meant that AVHRR statistics for large areas or large times required excessive amounts of data processing time. These limitations restricted the evaluation of the SMMR geophysical parameter retrieval in both time and area.

Open ocean buoy observations from FGGE buoys for 1979 have recently been obtained, and the AVHRR SST's are being reprocessed to eliminate duplicate observations. If a full year of SMMR T_b data becomes available, or if T_b's can be determined from the existing year of SMMR T_a data, a considerably more detailed and comprehensive evaluation of the SMMR data can be undertaken.